Electronic Supporting Information for

Oxo-functionalized mesoionic NHC nickel complexes for selective electrocatalytic reduction of CO_2 to formate

Simone Bertini,[a] Motiar Rahaman,[a] Abhijit Dutta,[a] Philippe Schollhammer,[b] Alexander V. Rudnev,[a,c] Fredric Gloaguen,*[,b] Peter Broekmann,*[,a] and Martin Albrecht*[,a]

(a) Department of Chemistry, Biochemistry &Pharmacy, Universität Bern, Freiestrasse 3, 3012 Bern (Switzerland)
(b) UMR 6521, CNRS, Université de Bretagne Occidentale, CS 93837, 29238 Brest (France)
(c) A.N. Frumkin Institute of Physical Chemistry and Electrochemistry Russian Academy of Sciences, Leninskii pr. 31, 119071 Moscow, Russia

Table of contents:

1. Ligand synthesis and characterisation..... S2
2. NMR data of all new compounds S8
3. Crystal data and structure refinement for complexes **3a–c**, **4**, **6a–b**..... S28
4. Cyclic voltammograms of complexes **3a–c**, **4**, **6a–b**..... S36
5. NMR and CV experiments in acidic media with complex **3a** S37
6. Electrocatalytic set-up and product quantification..... S39
7. Electrode surface characterisation after electrolysis with complex **6b**..... S49
8. References..... S50

1. Ligand synthesis and characterisation

General. 2-azidophenol **1,** 1-(2-phenol)-imidazole **8** and 2-amino-4,6-di-tertbutylphenol were synthesised following procedures reported in literature.[S1] All other reagents were commercially available and used as received. Unless stated otherwise, NMR spectra were recorded at 25 °C with Bruker spectrometers operating at 300 or 400 MHz (^{1}H NMR), and 100 MHz (^{13}C NMR), respectively. Chemical shifts (δ in ppm, coupling constants J in Hz) were referenced to residual solvent signals (^{1}H, ^{13}C). Assignments are based on homo- and heteronuclear shift correlation spectroscopy. The purity of bulk samples of the complexes has been established by NMR spectroscopy, and by elemental analysis, which were performed at the University of Bern Microanalytic Laboratory by using a Thermo Scientific Flash 2000 CHNS-O elemental analyzer. Residual solvent was confirmed by NMR spectroscopy and also by X-ray structure determinations. High-resolution mass spectrometry was carried out with a Thermo Scientific LTQ Orbitrap XL (ESI-TOF).

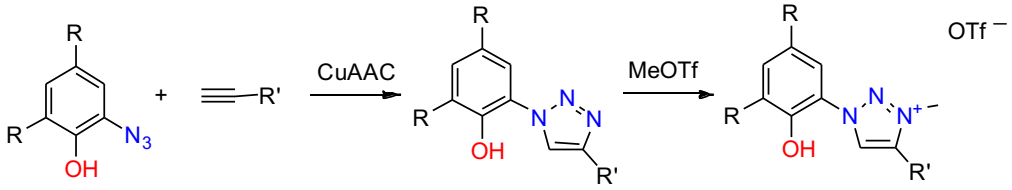

1: R=H
1^{Me}: R=Me
1^{tBu}: R=*t*Bu

7a: R=H, R'= Bu
7b: R=H, R'=Ph
7c: R=H, R'=Mes
7a^{Me}: R=Me, R'= Bu
7a^{tBu}: R=*t*Bu, R'=Bu

2a: R=H, R'= Bu
2b: R=H, R'=Ph
2c: R=H, R'=Mes
5a: R=Me, R'= Bu
5b: R=*t*Bu, R'=Bu

*Synthesis of 2-azido-4,6-di-methylphenol (**1**^{Me}).* 2-amino-4,6-di-methylphenol (500 mg, 3.65 mmol) was suspended in water and the rbf cooled to 0 ºC. Concentrated HCl (5 mL, 37% w/w) was added to the solution and stirred for 10 min. An aqueous solution of sodium nitrite (280 mg in 5 mL, 4.06 mmol) was then added dropwise over 10 min. After additional 30 min stirring, a sodium azide aqueous solution (300 mg in 10 mL, 4.61 mmol) was added dropwise to the reaction mixture and left stirring for 5 h at 0 ºC. After that time, Et_2O was added to the reaction (30 mL) and the 2 phases separated. The organic phase was washed with water (3 × 10 mL) and then dried over $MgSO_4$. The solvent was removed and the resulting oil was then purified by column chromatography (SiO_2; Et_2O/CH_2Cl_2 5:1) to leave 580 mg (96%) of ***1***^{Me} as a dark red oil. ^{1}H NMR (400 MHz, $CDCl_3$): δ 6.70 (s, 2H, 2 × H_{Ph}), 5.13 (s, 1H, OH), 2.23, 2.17 (2 × s, 3H, $ArCH_3$). $^{13}C\{^1H\}$ NMR (101 MHz, $CDCl_3$): δ 143.29 (C–O), 130.04 (C_{Ph}), 128.28 (C_{Ph}–H), 125.17 (C_{Ph}), 125.07 (C_{Ph}), 116.03 (C_{Ph}–H), 20.76 ($ArCH_3$), 15.69 ($ArCH_3$). HR-MS (ESI): calcd for $C_8H_9N_3O$ $[M–N]^+$ m/z = 151.0866 (found 151.1228).

*Synthesis of 2-azido-4,6-di-tertbutylphenol (**1**^{tBu}).* 2-amino-4,6-di-tertbutylphenol (760 mg, 3.4 mmol) was suspended in water and cooled to 0 ºC. H_2SO_4 (10 mL) was added to the solution and stirred

for 10 min. An aqueous solution of sodium nitrite (600 mg in 10 mL) was then added dropwise over 10 min. After additional 30 min stirring, a sodium azide aqueous solution (910 mg in 10 mL) was added dropwise to the reaction mixture and left stirring for 5 h at 0 ºC. After that time, Et_2O was added to the reaction (100 mL) and the two phases separated. The organic phase was washed with water (3 × 100 mL) and then dried over $MgSO_4$. The solvent was removed and the resulting oil was then purified by column chromatography (SiO_2; Et_2O/CH_2Cl_2 5:1) to leave 660 mg (82%) of ***1^{tBu}*** as dark red oil. ^{1}H NMR (300 MHz, $CDCl_3$): δ 7.05 (d, J = 2.1 Hz, 1H, H_{PhO}), 6.92 (d, J = 2.1 Hz, 1H, H_{PhO}), 5.44 (s, 1H, OH), 1.36, 1.28 (2 × s, 9H, CMe_3). $^{13}C\{^1H\}$ NMR (75 MHz, $CDCl_3$): δ 143.57 (C_{Ph}–O), 143.03 (C_{Ph}), 136.28 (C_{Ph}), 125.24 (C_{Ph}), 120.69 (C_{Ph}–H), 112.57 (C_{Ph}–H), 35.18, 34.77 (2 × CMe_3), 31.64, 29.48 (2 × C(*C*H_3)$_3$). HR-MS (ESI): calcd for $C_{14}H_{21}N_3O$ $[M+Na]^+$ m/z = 270.1513 (found 270.1524).

*Synthesis of 1-phenol-4-butyl-1,2,3-triazole (**7a**)*. 2-azidophenol 1 (250 mg, 1.85 mmol), 1-hexyne (236 mg, 2.3 mmol) and $CuSO_4 \cdot 5H_2O$ (80 mg, 0.28 mmol) were suspended in H_2O (10 mL). $N_2H_4.H_2O$ (0.1 mL) was added dropwise leading to the formation a dark grey precipitate. The mixture was stirred for 16 h, filtered, and the solid residue extracted with CH_2Cl_2 (3 × 10 mL). The organic solution was washed with dilute NH_4OH 30% (3 × 10 mL), with H_2O (15 mL), and finally with brine (10 mL). The organic layer was dried over Na_2SO_4, and evaporated to dryness. The residue was purified by column chromatography (Al_2O_3; CH_3CN/CH_2Cl_2 1:1) to yield the triazole **7a** as a grey powder (331 mg, 73%). ^{1}H NMR (400 MHz, $CDCl_3$): δ 10.07 (s, 1H, OH), 7.84 (s, 1H, H_{Trz}), 7.38 (dd, J = 8.8 Hz, 2.1 Hz, 1H, H_{PhOH}), 7.28 (td, J = 8.8, 2.1 Hz, 1H, H_{PhOH}), 7.18 (dd, J = 8.8, 2.1 Hz, 1H, H_{PhOH}), 6.98 (td, J = 8.8 Hz, 2.1 Hz, 1H, H_{PhOH}), 2.83 (t, J = 7.5 Hz, 2H, CH_2–Pr), 1.74–1.52 (m, 2H, CH_2–Et), 1.44–1.22 (m, 2H, CH_2–Me), 0.97 (t, J = 7.5 Hz, 3H, $(CH_2)_3$–C*H*$_3$). $^{13}C\{^1H\}$ NMR (101 MHz, $CDCl_3$): δ 149.51 (C–OH), 148.67 (C_{trz}–Bu), 129.50, 122.94, 120.18, 119.59 (4 × C_{PhOH}–H), 119.23 (C_{PhOH}–N), 118.66 (C_{trz}–H), 31.49 (CH_2–Pr), 25.38 (CH_2–Et), 22.42 (CH_2–Me), 13.93 (($CH_2)_3$–CH_3). HR-MS (ESI): calcd for $C_{12}H_{15}N_3O$ $[M+H]^+$ m/z = 218.1293 (found 218.1289).

*Synthesis of 1-phenol-4-(2-phenyl)-1,2,3-triazole (**7b**).* 2-azidophenol 1 (250 mg, 1.85 mmol), phenylacetylene (236 mg, 2.30 mmol) and $CuSO_4 \cdot 5H_2O$ (80 mg, 0.28 mmol) were suspended in a 1:1:1 v/v *t*BuOH/THF/H_2O solvent mixture (12 mL) and $N_2H_4.H_2O$ (0.1 mL) was added dropwise. The pale yellow solution was stirred for 16 h at room temperature (RT). All volatiles were removed in vacuo and the solid was extracted with MeOH (3 × 30 mL). The extracts were evaporated to dryness and the residue was purified by column chromatography (Al_2O_3; CH_3CN/CH_2Cl_2 1:2) to yield the triazole **7b** as an off-white powder (350 mg, 80%). ^{1}H NMR (400 MHz, DMSO–d_6): δ 10.57 (s, 1H, OH), 8.91 (s, 1H, H_{trz}), 7.95 (dd, J = 7.8, 2.0 Hz, 2H, H_{Ph}), 7.62 (dd, J = 8.8, 2.1 Hz, 1H, H_{PhOH}), 7.49 (td, J = 7.8, 2.1 Hz, 2H, H_{Ph}), 7.40–7.36 (m, 2H, H_{Ph} + H_{PhOH}), 7.14 (dd, J = 8.8, 2.1 Hz, 1H, H_{PhOH}) 6.99 (td, J =8.8, 2.1

Hz, 1H, H_{PhOH}). $^{13}C\{^1H\}$ NMR (101 MHz, DMSO–d_6): δ 149.86 (C–OH), 145.91 (C_{trz}–Ph), 130.38 (C_{PhOH}–N), 130.20 (C_{PhOH}–H), 128.75 (C_{PhOH}–H), 127.79 (C_{Ph}–H), 125.40 (C_{PhOH}–H), 125.13 (C_{Ph}–H), 124.40 (C_{Ph}–trz), 122.87 (C_{Trz}–H), 119.32 (C_{PhOH}–H), 116.82 (C_{Ph}–H). HR-MS (ESI): calcd for $C_{14}H_{11}N_3O$ $[M+H]^+$ m/z = 238.0975 (found 238.0973).

*Synthesis of 1-phenol-4-mesityl-1,2,3-triazole (**7c**).* 2-azidophenol 1 (250 mg, 1.85 mmol), mesitylacetylene (236 mg, 2.30 mmol) and $CuSO_4 \cdot 5H_2O$ (80 mg, 0.28 mmol) were suspended in a 1:1:1 v/v *t*BuOH/THF/H_2O solvent mixture (12 mL) and $N_2H_4.H_2O$ (0.1 mL) was added dropwise. The pale yellow solution was stirred for 16 h, during which time a dark grey precipitate formed gradually. All volatiles were removed in vacuo and the solid was extracted with MeOH (3 × 30 mL). The extracts were evaporated to dryness and the residue was purified by column chromatography (Al_2O_3; CH_3CN/CH_2Cl_2 1:2) to yield triazole **7c** as a grey powder (350 mg, 80%). ^1H NMR (400 MHz, DMSO-d_6): δ 10.51 (br s, OH), 8.49 (s, 1H, H_{trz}), 7.69 (dd, J = 8.2 , 2.1 Hz, 1H, H_{PhOH}), 7.36 (td, J = 8.2, 2.1 Hz, 1H, H_{PhOH}), 7.12 (dd, J = 8.2, 2.1 Hz, 1H, H_{PhOH}), 7.08–6.92 (m, 3H, $2H_{Mes}$ + H_{PhOH}), 2.29 (s, 3H, CH_3–Mes), 2.12 (s, 6H, CH_3–Mes). $^{13}C\{^1H\}$ NMR (101 MHz, DMSO d6): δ 149.72 (C–OH), 143.68 (C_{trz}–Mes), 137.20, 137.04, 129.99, 128.16 (4 × C_{PhOH}–H), 127.27 (C_{Mes}–H), 125.40 (C_{trz}–H), 125.11 (C_{Mes}–Trz), 124.66 (C_{Mes}–CH_3), 119.45 (C_{Mes}–CH_3), 117.05 (C_{PhOH}–N), 20.64 (CH_3–Mes), 20.42 (CH_3–Mes). HR-MS (ESI): calcd for $C_{17}H_{17}N_3NaO$ $[M+Na]^+$ m/z = 302.1264 (found 302.1266).

*Synthesis of 2-(4-butyl-1H-1,2,3-triazol-1-yl)-4,6-dimethylphenol (**7^{Me}**).* To a solution of **1^{Me}** (500 mg; 3.06 mmol) in THF (15 ml) $CuSO_4 \cdot 5H_2O$ (180 mg; 0.75 mmol), 1-hexyne (266 mg; 3.25 mmol) sodium ascorbate (0.73 g; 3.76 mmol) and H_2O (15 mL) were added and the reaction mixture was stirred at 70 °C for 16 h. After this time, the THF was removed *in vacuo* and the solid redissolved in CH_2Cl_2. The organic solution was washed with dilute NH_4OH solution (4 × 15 mL), H_2O (20 mL) and brine (15 mL) and dried over $MgSO_4$. The solution filtered through a short pad of silica and eluted with CH_2Cl_2. All volatiles were removed under reduced pressure. Product **7^{Me}** was obtained in high purity by column chromatography (SiO_2; CH_2Cl_2) as a red oil (615 mg, 82%).^1H NMR (400 MHz, $CDCl_3$): δ 9.91 (s, 1H, –OH), 7.76 (s, 1H, H_{Trz}), 6.97 (s, 1H, H_{PhO}), 6.92 (d, 1H, H_{PhO}), 2.77 (t, J = 6.0 Hz, 2H, CH_2–Pr), 2.27, 2.26 (2 × s, 3H, $ArCH_3$), 1.73–1.65 (m, 2H, CH_2–Et), 1.44–1.34 (m, 2H, CH_2–Me), 0.93 (t, J = 6.0 Hz, 3H, $(CH_2)_3$–CH_3). $^{13}C\{^1H\}$ NMR (101 MHz, $CDCl_3$): δ 148.44 (C–O), 145.38 (C_{Ph}), 131.38 (C_{Ph}–H), 128.85 (C_{Ph}), 128.47 (C_{Ph}–H), 122.10 (C_{Trz}–Bu), 118.85 (C_{Trz}–H), 117.14 (C_{Ph}–H), 31.46 (CH_2–Pr), 25.35 (CH_2–Et), 22.38 (CH_2–CH_3), 20.57 (CH_3), 16.37 (CH_3), 13.91 (CH_3). HR-MS (ESI): calcd for $C_{14}H_{19}N_3O$ $[M+H]^+$ m/z = 246.1601 (found 246.1600).

*Synthesis of 2-(4-butyl-1H-1,2,3-triazol-1-yl)-4,6-di-tertbutylphenol (**7^{tBu}**).* To a solution of **1^{tBu}** (318 mg, 1.29 mmol), $CuSO_4 \cdot 5H_2O$ (90 mg; 0.38 mmol), 1-hexyne (130 mg; 1.60 mmol) sodium ascorbate (0.37 g; 1.86 mmol) and H_2O (15 mL) were added and the reaction mixture was stirred at 70 °C for 16 h. were added to an acetone/H_2O (20/10 mL) mixture and left stirring for 16 hours at 80°C. After that time, all solvents were evaporated from the resulting suspension. CH_2Cl_2 (50 mL) was then added to the solid and the reaction mixture was filtered through celite. The organic fraction was washed with water (3 × 50 ml) and then dried with Na_2SO_4. Product **7^{tBu}** was obtained in high purity by column chromatography (SiO_2; CH_2Cl_2/Et_2O 1:3) as a red oil (320 mg, 75%). ^{1}H NMR (300 MHz, $CDCl_3$): δ 9.98 (s, 1H, –OH), 7.75 (s, 1H, H_{Trz}), 7.32 (d, J = 2.1 Hz, 1H, H_{PhO}), 7.13 (d, J = 2.1 Hz, 1H, H_{PhO}), 2.79 (t, J = 6.0 Hz, 2H, CH_2–Pr), 1.74–1.66 (m, 2H, CH_2–Et), 1.44–1.32 (m, 11H, $(CH_3)_3$–C + CH_2–Me), 1.31 (s, 9H, $C(CH_3)_3$), 0.94 (t, J = 6.0 Hz, 3H, $(CH_2)_3$–C*H*$_3$). ^{13}C{^{1}H} NMR (75 MHz, $CDCl_3$): δ 148.53 (C–O), 146.18, 142.01, 139.21 (3 × C_{Ph}), 124.15 (C_{Ph}–H), 122.94 (C_{Trz}–Bu), 119.67 (C_{Trz}–H), 114.68 (C_{Ph}–H), 35.76, 34.54 (2 × CMe_3), 31.60 (C(*C*H$_3$)$_3$ + CH_2–Pr), 29.60 (C(*C*H$_3$)$_3$), 25.42 (CH_2–Et), 22.46 (CH_2–Me), 13.96 ($(CH_2)_3$–*C*H$_3$). HR-MS (ESI): calcd for $C_{20}H_{32}N_3O$ $[M+H]^+$ m/z = 330.2540 (found 330.2547).

*General procedure for synthesis of triazolium salts **2a–c***. The triazole was dissolved in CH_2Cl_2 (10 mL) and MeOTf (1.2 eq) was added. After stirring for 1 h at RT, all volatile components were removed. The pure triazolium salt was obtained after column chromatography (basic Al_2O_3; CH_3CN/CH_2Cl_2 1:2).

*Synthesis of 1-(2-hydroxyphenyl)-3-methyl-4-butyl-1H-1,2,3-triazolium triflate (**2a**).* The compound was prepared according to the general procedure from compound **7a** (330 mg, 1.5 mmol) and MeOTf (275 mg, 1.7 mmol), yielding **7a** as a grey highly hygroscopic powder (518 mg, 94%). ^{1}H NMR (400 MHz, $CDCl_3$): δ 8.45 (s, 1H, H_{trz}), 7.54 (dd, J = 8.8, 2.1 Hz, 1H, H_{PhOH}), 7.30 (td, J = 8.8, 1H, H_{PhOH}), 7.18 (dd, J = 8.8, 2.1 Hz, 1H, H_{PhOH}), 6.88 (td, J = 8.8, 2.1 Hz, 1H, H_{PhOH}), 4.26 (s, 3H, CH_3–N), 2.84 (t, J = 7.5 Hz, 2H, CH_2–Pr), 1.68 (quintet, J = 7.5 Hz, 2H, CH_2–Et), 1.43 (sextet, J = 7.5 Hz, 2H, CH_2–Me), 0.93 (t, J = 7.5 Hz, 3H, $(CH_2)_3$–C*H*$_3$). ^{13}C{^{1}H} NMR (101 MHz, $CDCl_3$): δ 149.87 (C–OH), 144.63 (C_{trz}–Bu), 133.05 (C_{PhOH}–H), 128.68 (C_{PhOH}–H), 124.14 (C_{PhOH}–H), 122.38 (C_{PhOH}–H), 120.73 (C_{PhOH}–N), 119.04 (C_{trz}–H), 37.89 (CH_3–N), 28.95 (CH_2–Pr), 23.26 (CH_2–Et), 22.26 (CH_2–Me), 13.61 ($(CH_2)_3$–*C*H$_3$). HR-MS (ESI): calcd for $C_{12}H_{15}ON_3$ $[M–OTf]^+$ m/z = 232.1444 (found 232.1443). Anal. Calcd for $C_{14}H_{18}F_3N_3O_4S$ (381.37): C, 44.09; H, 4.76; N, 10.02; S, 8.41. Found: C, 43.84; H, 5.18; N, 10.15; S, 9.05%.

*Synthesis of 1-(2-hydroxyphenyl)-3-methyl-4-phenyl-1H-1,2,3-triazolium triflate (**2b**).* The compound was prepared according to the general procedure from **7b** (350 mg, 1.5 mmol) and MeOTf (264 mg, 1.6 mmol), yielding **7b** as an off-white and highly hygroscopic powder (394 mg, 60%). ^{1}H NMR (400 MHz,

CD_3CN): δ 8.89 (s, 1H, H_{trz}), 7.73–7.60 (m, 6H, $5H_{Ph}$ + $1H_{PhOH}$), 7.57 (td, J = 9.0 Hz, 2.2 Hz 1H, H_{PhOH}), 7.31 (dd, J = 9.0, 2.2 Hz 1H, $2H_{PhOH}$), 7.14 (td, J = 9.0, 2.2 Hz, 1H, H_{PhOH}), 4.29 (s, 3H, N–CH_3). $^{13}C\{^1H\}$ NMR (101 MHz, CD_3CN): δ 151.02 (C–OH), 144.09 (C_{trz}–Ph), 134.28 (C_{PhOH}–N), 132.83 (C_{Ph}–H), 130.78 (C_{Ph}–H), 130.56, 130.54,126.36 (3 × C_{PhOH}–H), 123.50 (C_{Ph}–C_{Trz}), 123.33 (C_{PhOH}–H), 121.90 (C_{trz}–H), 118.82 (C_{PhOH}–H), 39.72 (N–CH_3). HR-MS (ESI): calcd for $C_{15}H_{14}N_3O$ $[M–OTf]^+$ m/z = 252.1131 (found 252.1126). Anal. Calcd for $C_{16}H_{14}F_3N_3O_4S$ (332.35): C, 47.88; H, 3.52; N, 10.46; S, 7.99. Found: C, 47.22; H, 4.00; N, 10.16; S, 8.40.

*Synthesis of 1-(2-hydroxyphenyl)-3-methyl-4-mesityl-1H-1,2,3-triazolium triflate (**2c**).* The compound was obtained according to the general procedure from **7c** (300 mg, 1.5 mmol) and MeOTf (250 mg, 1.7 mmol), yielding **2c** as an off-white powder (500 mg, 94%). ^1H NMR (400 MHz, $CDCl_3$): δ 9.18 (s, 1H, H_{trz}), 7.75 (dd, J = 8.5, 2.0 Hz 1H, H_{PhOH}), 7.53 (dd, J = 8.5, 2.0 Hz, 1H, H_{PhOH}), 7.30 (td, J = 8.5, 2.0 Hz, 1H, H_{PhOH}), 7.01 (s, 2H, H_{Mes}), 6.86 (td, J = 8.5, 2.0 Hz, 1H, H_{PhOH}), 4.06 (s, 3H, CH_3–N), 2.31 (s, 3H, CH_3–Mes), 2.04 (s, 6H, CH_3–Mes).$^{13}C\{^1H\}$ NMR (101 MHz, $CDCl_3$): δ 152.55 (C–OH), 142.79 (C_{trz}–Mes), 141.26, 138.12, 133.02, 129.88 (4 × C_{PhOH}–H), 129.50 (C_{Mes}–H), 122.78 (C_{trz}–H), 122.26 (C_{Mes}–Trz), 120.05 (C_{Mes}–CH_3), 118.73 (C_{Mes}–CH_3), 117.47 (C_{PhOH}–N), 37.62 (CH_3–N), 21.31 (CH_3–Mes), 20.15 (CH_3–Mes). HR-MS (ESI): calcd for $C_{18}H_{20}N_3O$ $[M–OTf]^+$ m/z = 294.1606 (found 294.1598). Anal. Calcd for $C_{19}H_{20}F_3N_3O_4S$: C, 51.46; H, 4.55; N, 9.48. Found: C, 51.10; H, 4.30; N, 9.40.

*Synthesis of 4-butyl-1-(2-hydroxy-3,5-dimethylphenyl)-3-methyl-1H-1,2,3-triazol-3-ium triflate (**5a**).* To a solution of $\mathbf{7^{Me}}$ (300 mg, 1.22 mmol) in CH_2Cl_2 (25 mL) was added MeOTf (0.14 mL, 1.2 mmol). After 2 h stirring at room temperature, the solvent was evaporated and the product purified by column chromatography (Al_2O_3; Et_2O/CH_2Cl_2 3:1) to afford **5a** as a pale red oil (450 mg, 90%). ^1H NMR (300 MHz, CDCN): δ 8.50 (s, 1H, H_{Trz}), 7.29 (s, 1H, H_{PhO}), 7.22 (s, 1H, H_{PhO}), 4.24 (s, 3H, CH_3), 2.91 (t, J = 6.0 Hz, 2H, CH_2–Pr), 2.33 (s, 6H, 2 ArCH_3), 1.81–1.71 (m, 2H, CH_2–Et), 1.54–1.47 (m, 2H, CH_2–Me), 1.01 (t, J = 6.0 Hz, 3H, $(CH_2)_3$–C*H*$_3$). $^{13}C\{^1H\}$ NMR (75 MHz, CD_3CN): δ 146.60 (C–O), 145.51 (C_{Ph}), 135.82 (C_{Ph}–H), 131.70 (C_{Trz}–H), 130.33 (C_{Ph}–H), 128.58 (C_{Ph}), 124.03 (C_{Trz}–Bu), 123.96 (C_{Ph}–H), 38.46 (CH_3–N), 29.52 (CH_2–Pr), 23.46 (CH_2–Et), 22.61 (CH_2–Me), 20.18 (($CH_2)_3$–CH_3), 16.70, 13.75 (2 × ArCH_3). HR-MS (ESI): calcd for $C_{16}H_{22}F_3N_3O_4S$ $[M–OTf]^+$ m/z = 260.1757 (found 260.1757). Anal. Calcd for $C_{16}H_{22}F_3N_3O_4S$ (409.42) : C, 46.94; H, 5.42; N, 10.26. Found: C, 46.63; H, 5.62; N, 10.24.

*Synthesis of 4-butyl-1-(3,5-di-tert-butyl-2-hydroxyphenyl)-3-methyl-1H-1,2,3-triazol-3-ium triflate (**5b**).* To a solution of $\mathbf{7^{tBu}}$ (300 mg, 0.91 mmol) in CH_2Cl_2 (20 mL) was added MeOTf (0.11 mL, 1.0

mmol). After 5 h stirring at room temperature, the solvent was evaporated and the product purified by column chromatography (Al_2O_3; Et_2O/CH_2Cl_2 3:1) to yield **5b** as a dark red oil (340 mg, 75%). ^{1}H NMR (400 MHz, $CDCl_3$): δ 8.14 (s, 1H, H_{Trz}), 7.86 (s, b, 1H, –OH), 7.50 (d, J = 2.1 Hz, 1H, H_{PhO}), 7.08 (d, J = 2.1 Hz, 1H, H_{PhO}), 4.29 (s, 3H, CH_3), 2.91 (t, J = 6.0 Hz, 2H, CH_2–Pr), 1.81–1.77 (m, 2H, CH_2–Et), 1.52–1.46 (m, 2H, CH_2–Me), 1.40, 1.28 (2 × s, 9H, $C(CH_3)_3$) 0.96 (t, J = 6.0 Hz, 3H, $(CH_2)_3$–CH_3). $^{13}C\{^1H\}$ NMR (100 MHz, $CDCl_3$): δ 147.31 (C–O), 145.54 (C_{Ph}), 143.83 (C_{Ph}), 141.88 (C_{Ph}), 129.15 (C_{Ph}–H), 127.90 (C_{Trz}–H), 124.53 (C_{Trz}–Bu), 119.79 (C_{Ph}–H), 35.94 (CH_3–N), 34.67, 34.26 (2 × CMe_3), 31.43, 29.72 (2 × $C(CH_3)_3$), 28.78 (CH_2–Pr), 23.52 (CH_2–Et), 22.37 (CH_2–Me), 14.19 $(CH_2)_3$–CH_3). HR-MS (ESI): calcd for $C_{22}H_{34}F_3N_3O_4S$ $[M–OTf]^+$ m/z = 344.2702 (found 344.2692). Anal. Calcd for $C_{22}H_{34}F_3N_3O_4S$ (493.59) : C, 53.54; H, 6.94; N, 8.51. Found: C, 53.61; H, 6.82; N, 8.24.

*Synthesis of 1-(2-phenol)-3-methyl-imidazolium iodide (**9**)*

8 **9**

250 mg (0.87 mmol) of 1-(2-phenol)-imidazole **8** was dissolved in CH_3CN (10 mL) and iodomethane (60 µL,0.96 mmol) was added. After stirring for 3 h at reflux temperature, the mixture was concentrated in vacuo to 1 mL. Precipitation with Et_2O (30 mL), filtration and subsequent drying in vacuo afforded the pure imidazolium salt **9** as a white powder (252 mg, 96%). ^{1}H NMR (300 MHz, CD_3OD): δ 9.30 (s,1H, H_{Im}), 7.88 (t, J = 2.0 Hz, 1H, H_{Im}), 7,74 (t, J = 2.0 Hz, 1H, H_{Im}), 7.50 (dd, J = 7.5, 1.9 Hz, 1H, H_{PhOH}), 7.42 (td, J = 7.5, 1.9 Hz, 1H, H_{PhOH}), 7.11 (dd, J = 7.5, 1.9 Hz, 1H, H_{PhOH}), 7.05 (td, J = 7.5, 1.9 Hz, 1H, H_{PhOH}), 4.04 (s, 3H, CH_3–N). $^{13}C\{^1H\}$ NMR (76 MHz, CD_3OD): δ 152.03 (C–O), 138.85 (C_{Im}), 132.67 (C_{PhO}–H), 126.48 (C_{PhO}–H), 124.72 (C_{Im}–H), 124.55 (C_{Im}–H), 123.81 (C_{PhO}–N), 118.15 (C_{imi}–H), 36.71 (CH_3–N). HR-MS (ESI): calcd for $C_{10}H_{11}N_2O^+$ $[M–I]^+$ m/z = 175.08659 (found 175.08661). Anal. Calcd for $C_{10}H_{11}IN_2O_2$ (404.08): C, 39.76; H, 3.67; N, 9.27. Found: C, 39.86; H, 3.55; N, 9.33.

2. NMR data of all new compounds

2-azido-4,6-di-methylphenol (1^{Me})

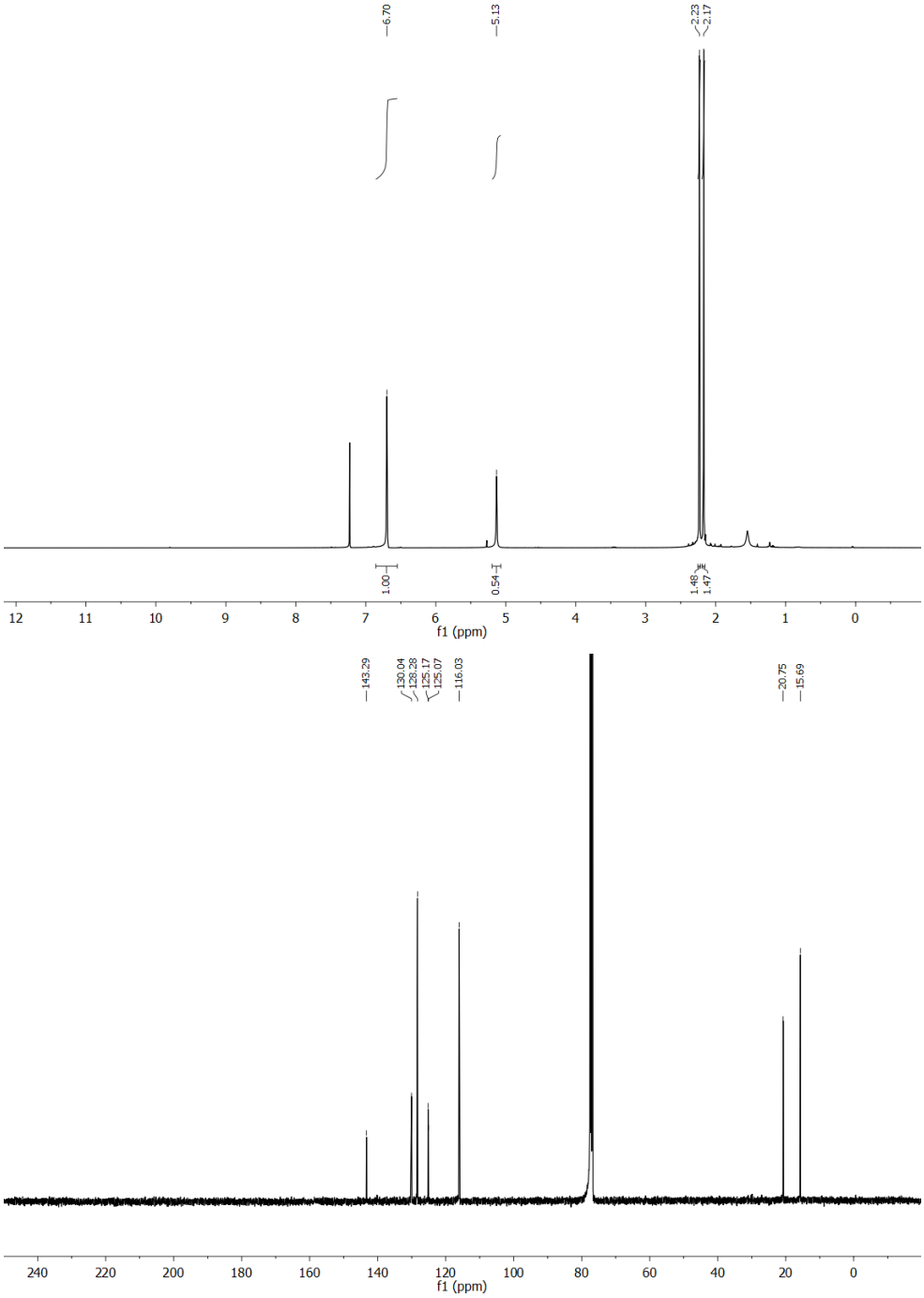

Figure S1. NMR spectra of $\mathbf{1^{Me}}$: top ^{1}H (400 MHz), bottom $^{13}C\{^{1}H\}$ (101 MHz) in $CDCl_3$.

2-azido-4,6-di-tertbutylphenol (1^{tBu})

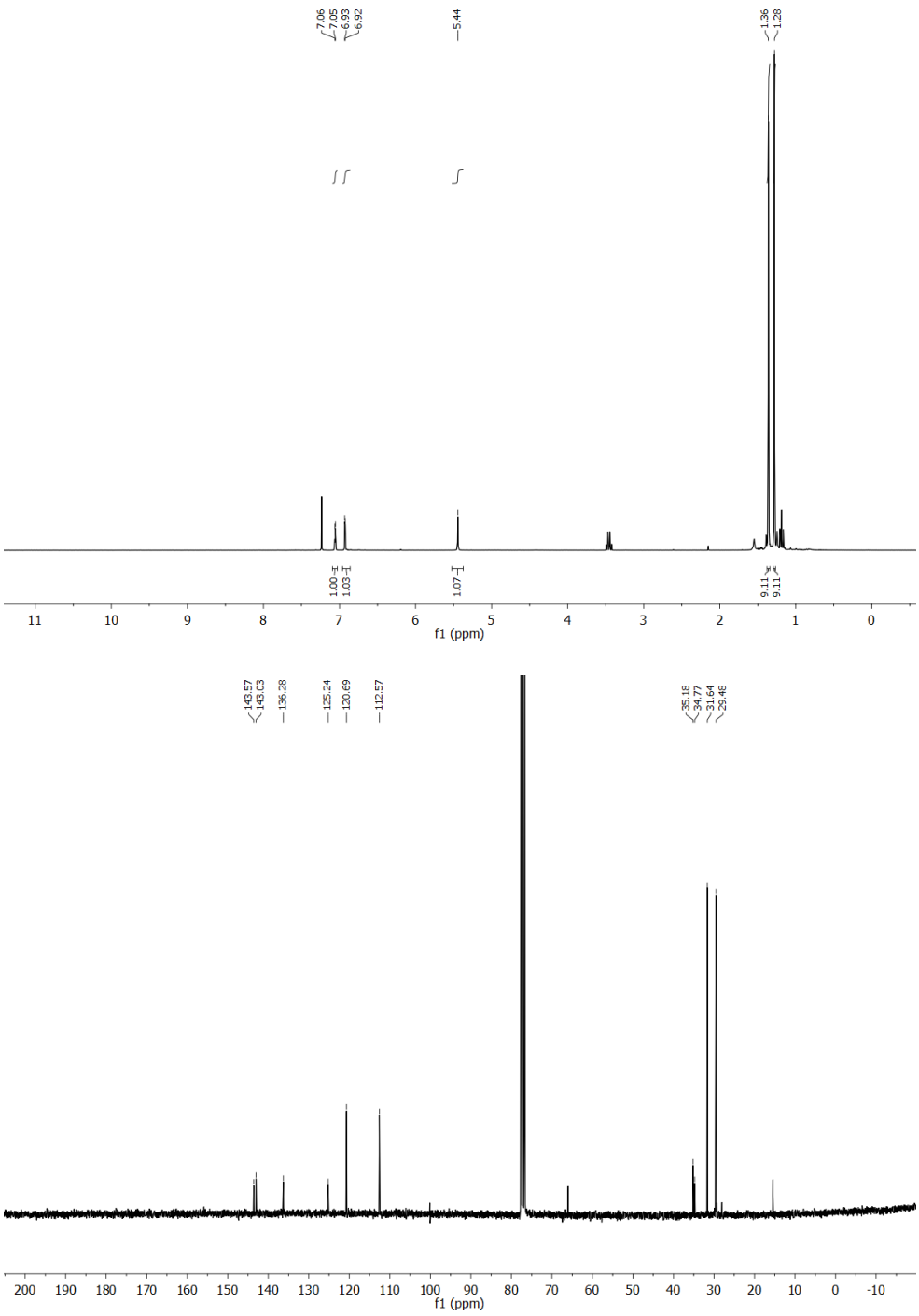

Figure S2. NMR spectra of $\mathbf{1^{tBu}}$: top ^{1}H (300 MHz), bottom $^{13}C\{^{1}H\}$ (75 MHz) in $CDCl_3$.

1-(2-hydroxyphenyl)-3-methyl-4-butyl-1H-1,2,3-triazolium triflate (2a)

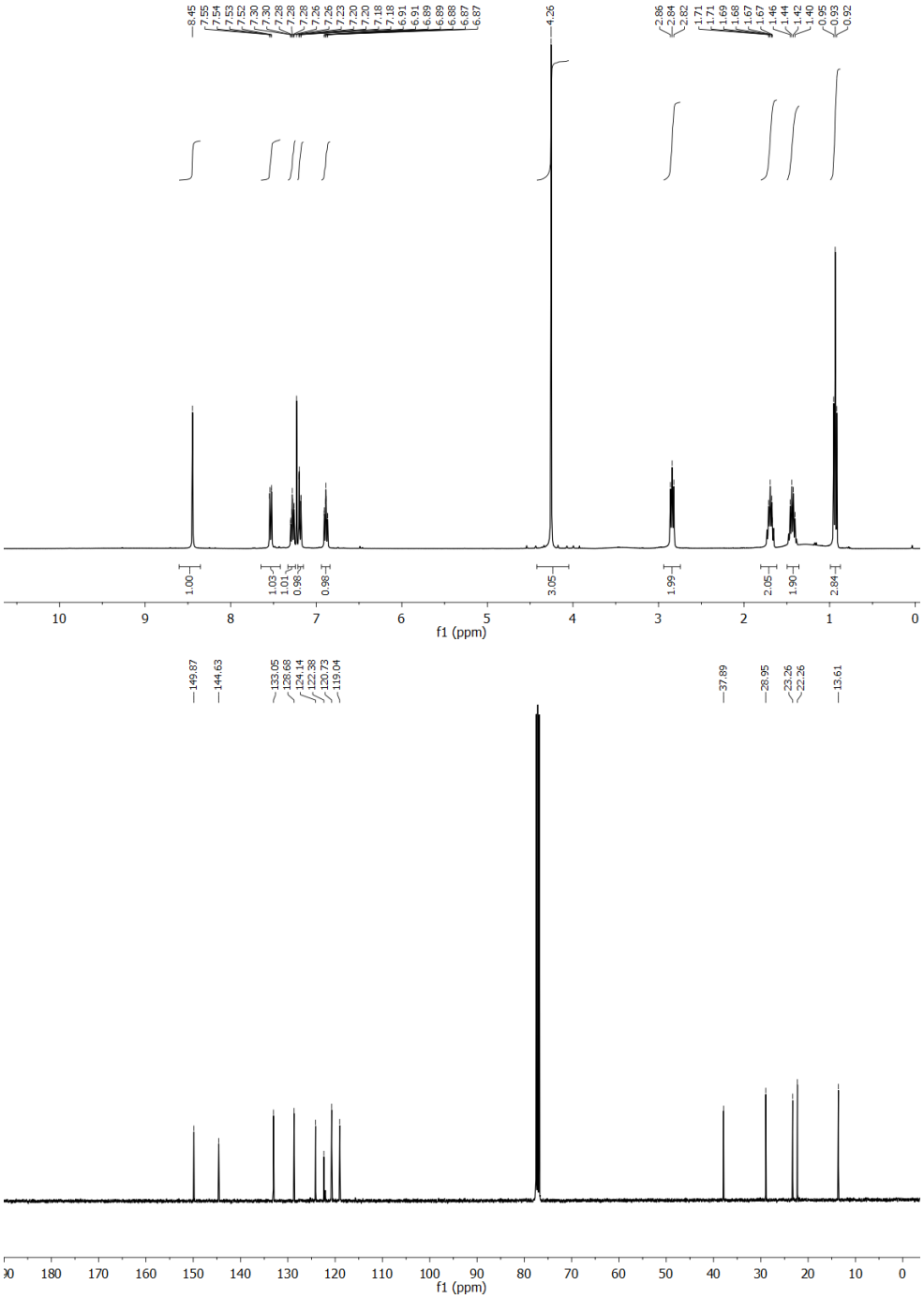

Figure S3. NMR spectra of **2a**: top ^{1}H (400 MHz), bottom $^{13}C\{^{1}H\}$ (101 MHz) in $CDCl_3$.

1-(2-hydroxyphenyl)-3-methyl-4-phenyl-1H-1,2,3-triazolium triflate (2b)

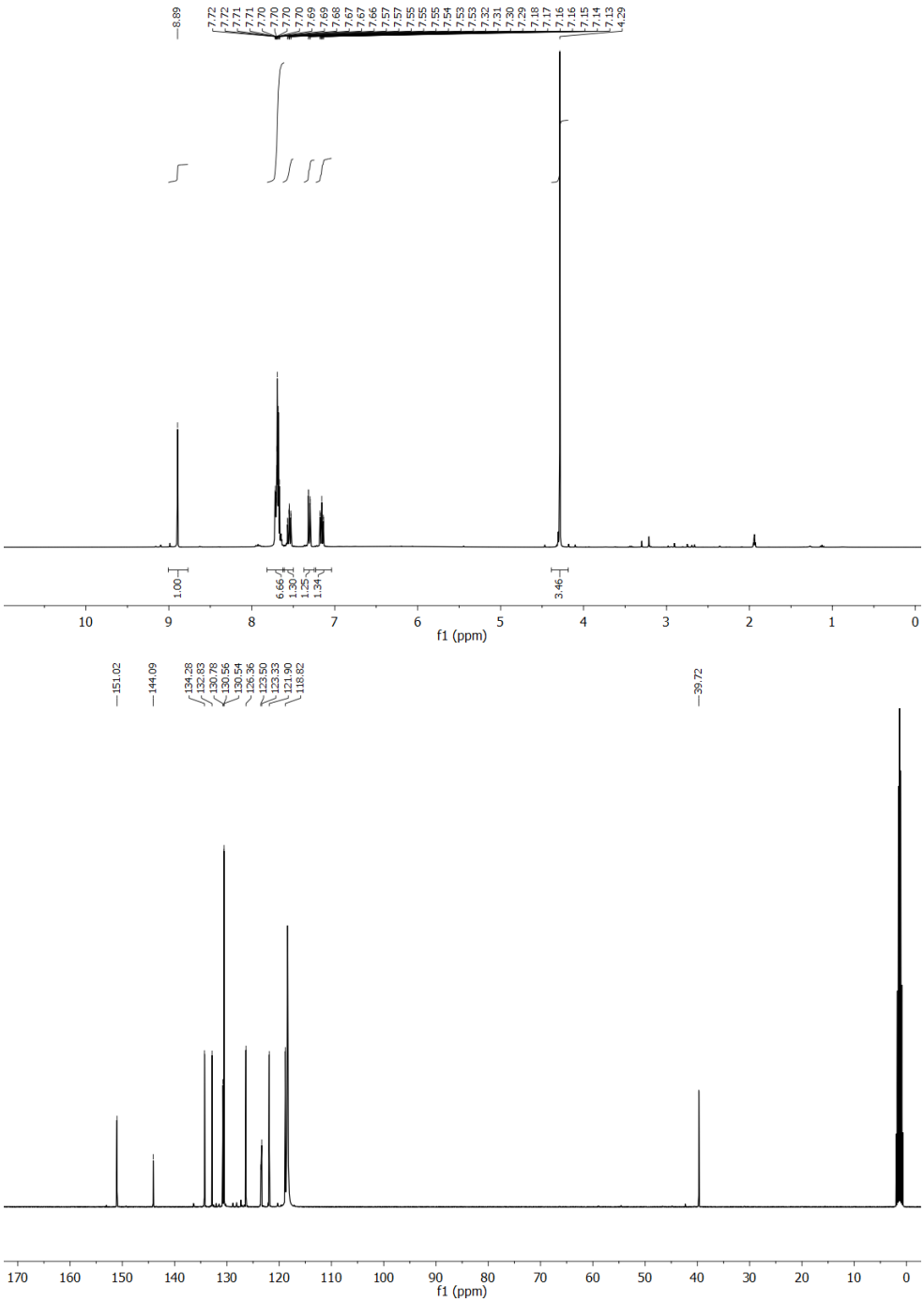

Figure S4. NMR spectra of **2b**: top ^{1}H (400 MHz), bottom $^{13}C\{^{1}H\}$ (101 MHz) in CD_3CN.

1-(2-hydroxyphenyl)-3-methyl-4-mesityl-1H-1,2,3-triazolium triflate (2c)

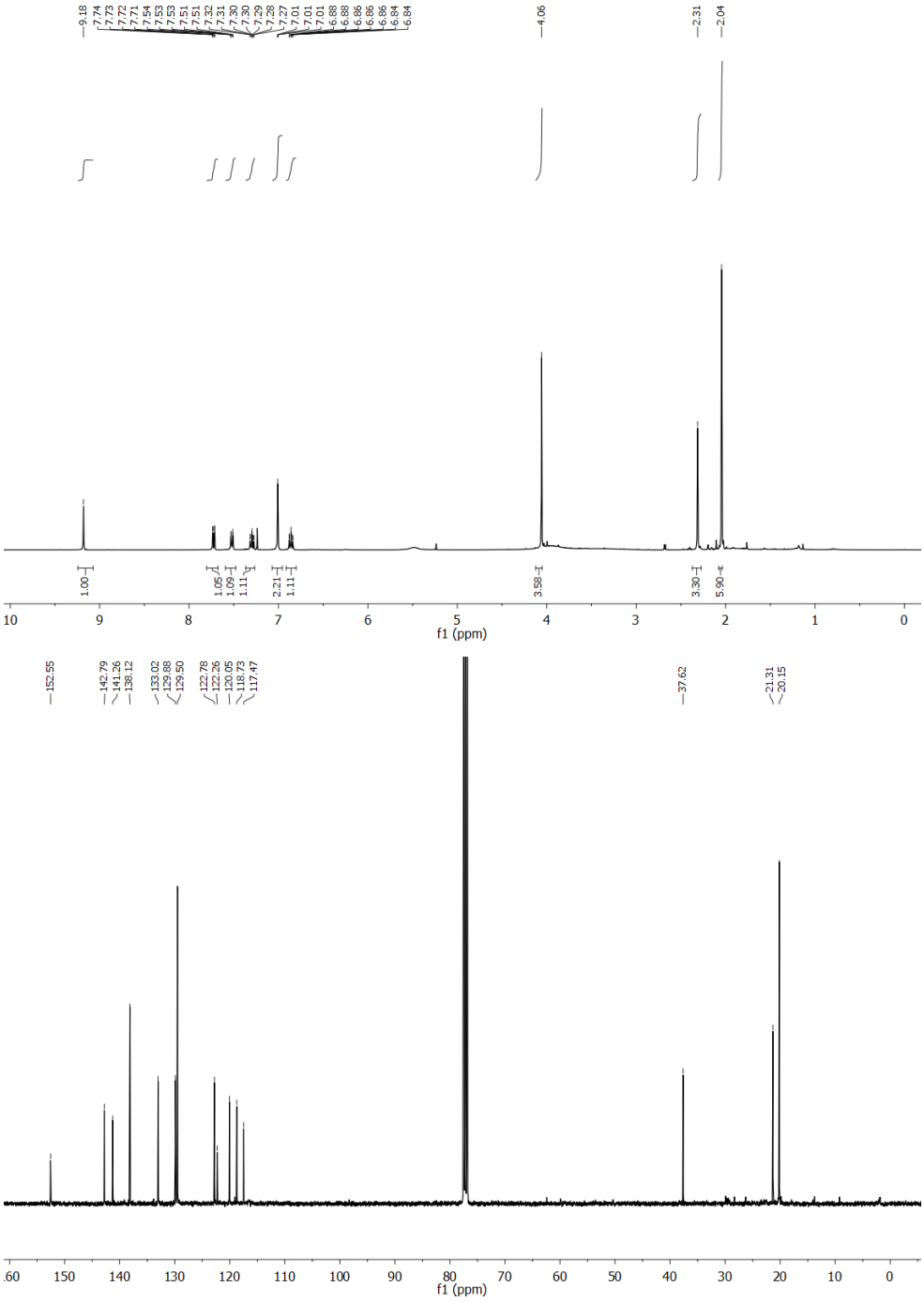

Figure S5. NMR spectra of **2c**: top ^{1}H (400 MHz), bottom $^{13}C\{^{1}H\}$ (101 MHz) in $CDCl_3$.

***cis*-[Ni(trz^{Bu}^OPh)$_2$] (3a)**

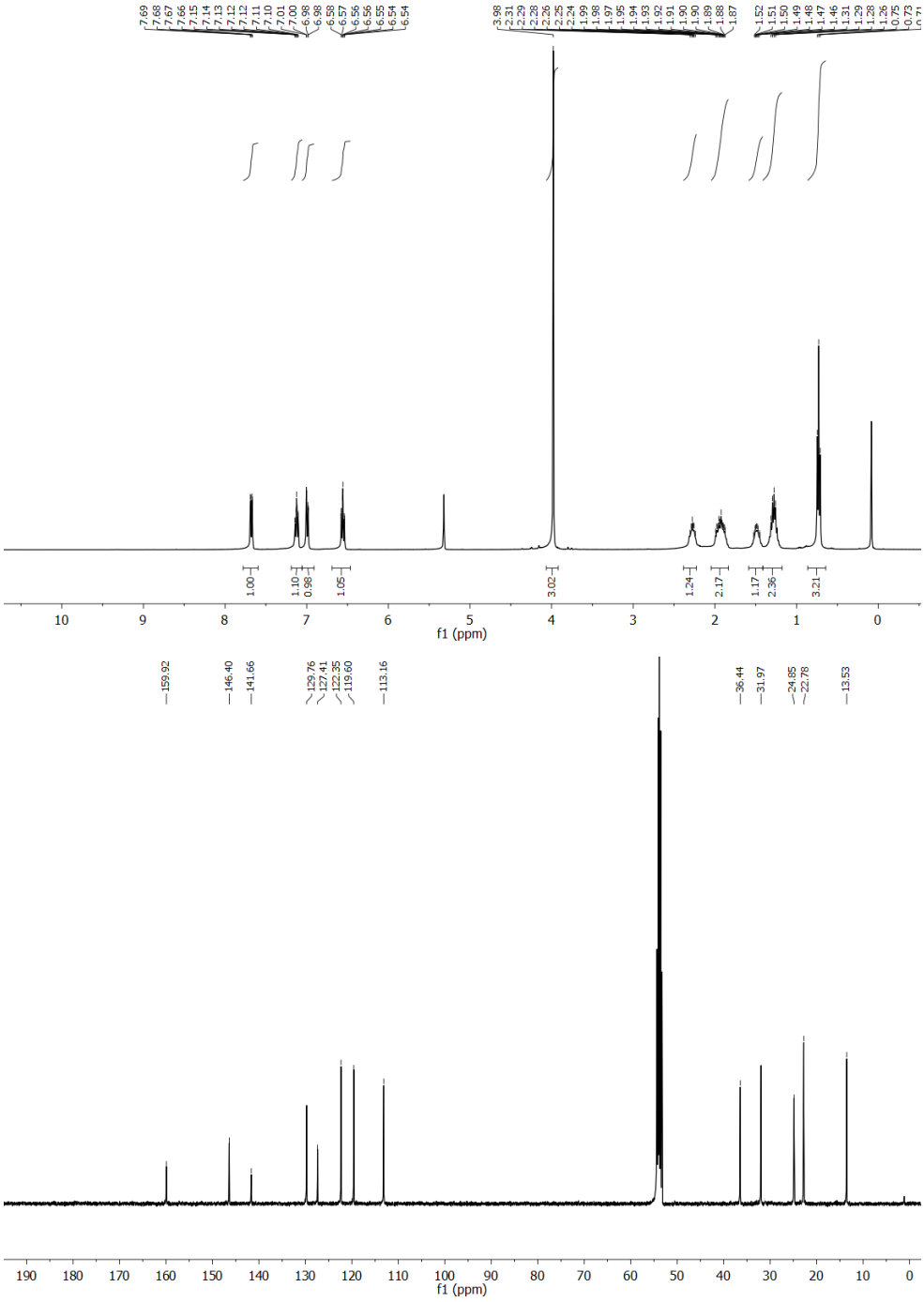

Figure S6. NMR spectra of **3a**: top ^{1}H (400 MHz), bottom ^{13}C{^{1}H} (101 MHz) in CD_2Cl_2.

***cis*-[Ni(trz^{Ph}^OPh)$_2$] (3b)**

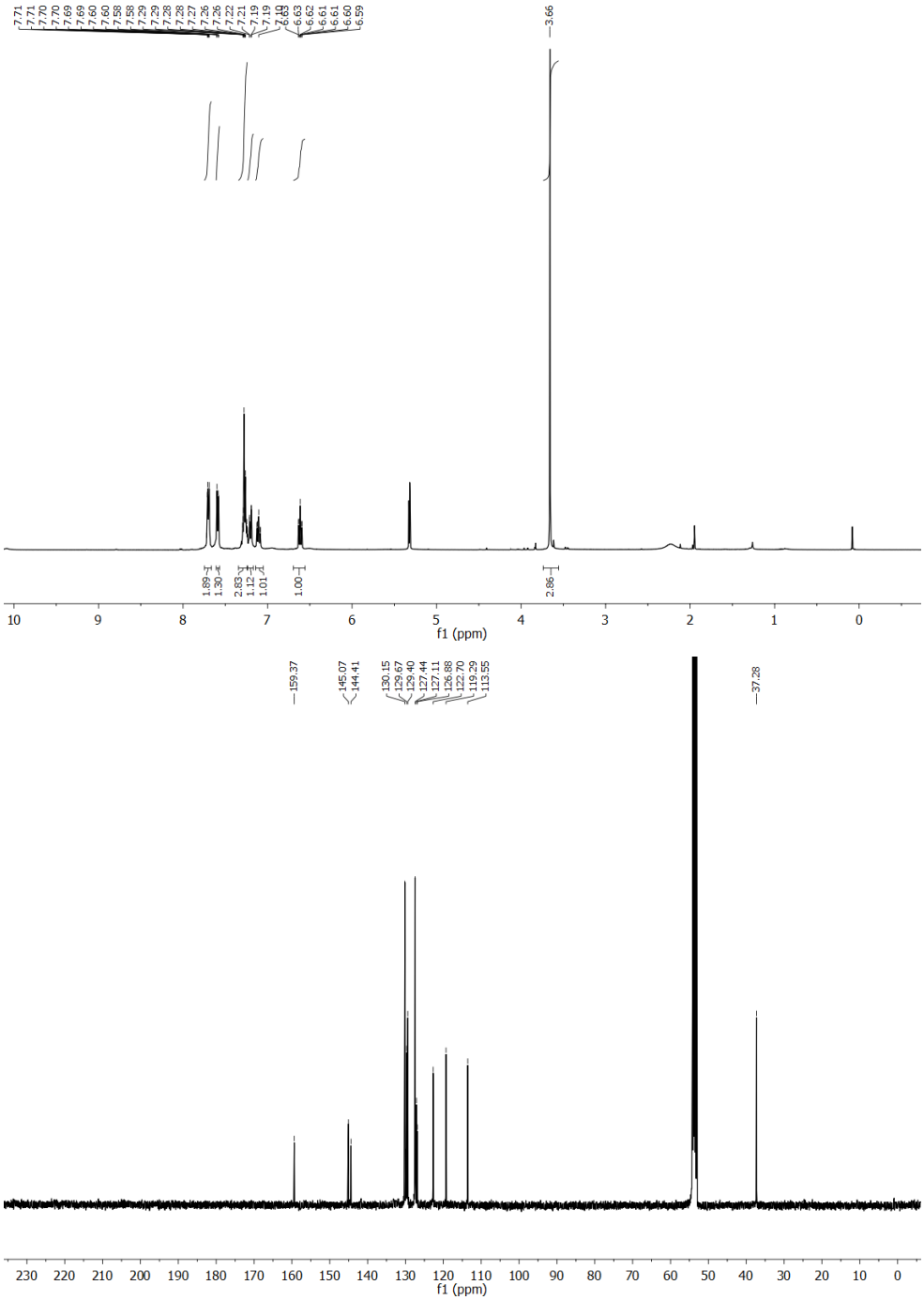

Figure S7. NMR spectra of **3b**: top ^{1}H (400 MHz), bottom ^{13}C{^{1}H} (101 MHz) in CD_2Cl_2.

***trans*-[Ni(trz^{Mes}^OPh)$_2$] (3c)**

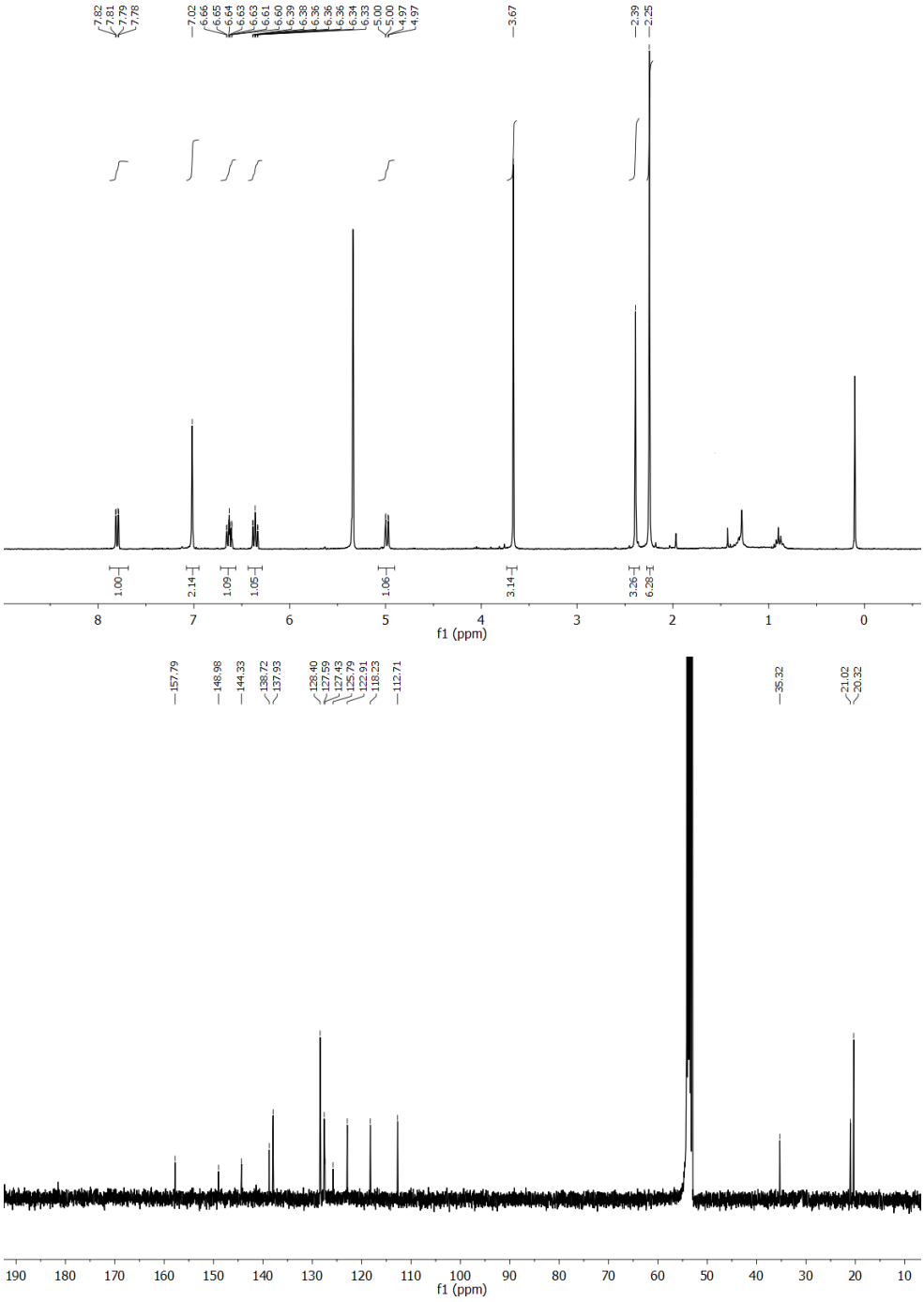

Figure S8. NMR spectra of **3c**: top ^{1}H (400 MHz), bottom ^{13}C{^{1}H} (101 MHz) in CD_2Cl_2.

***cis*-[Ni(Im^OPh)$_2$] (4)**

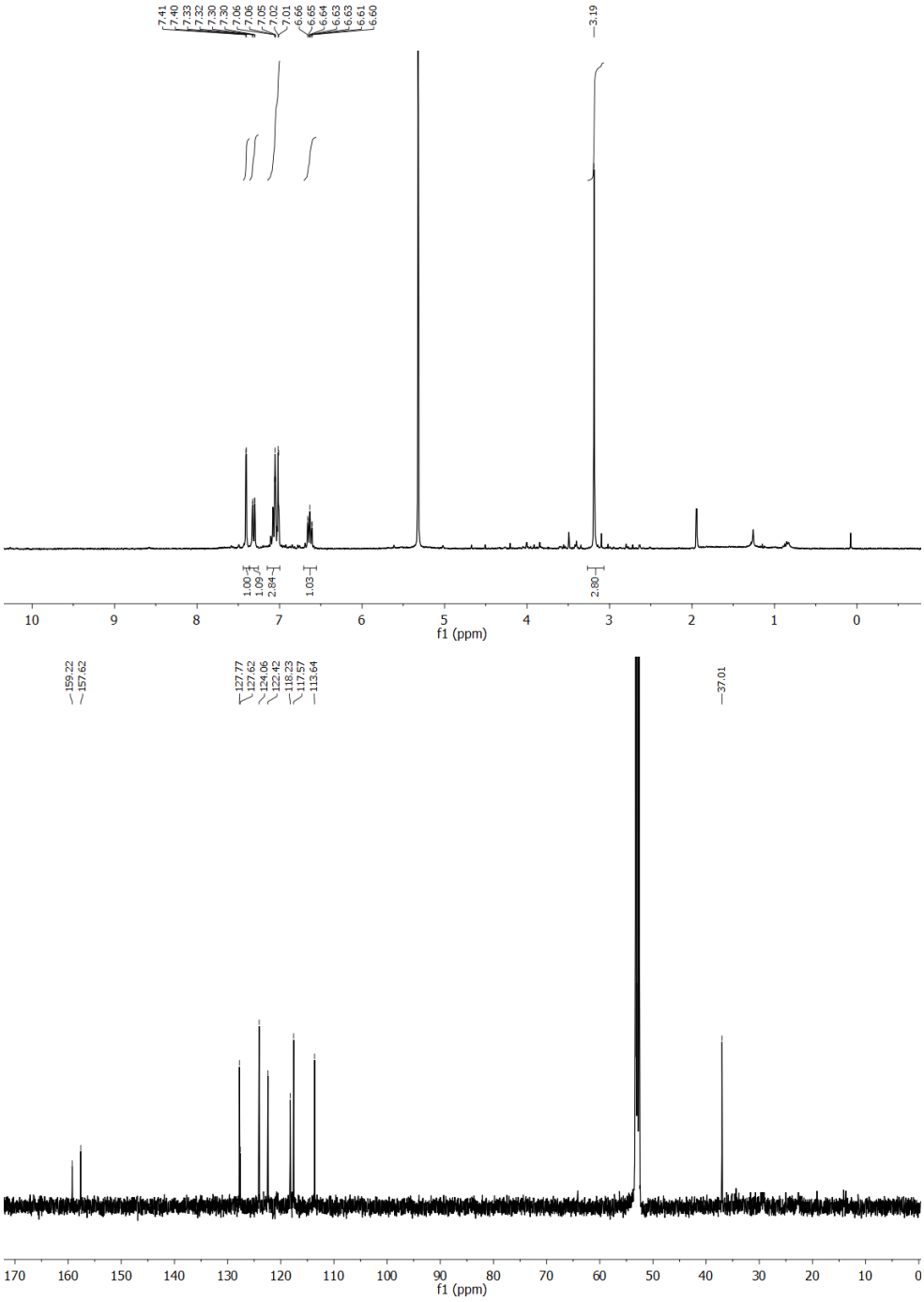

Figure S9. NMR spectra of **4**: top ^{1}H (400 MHz), bottom ^{13}C{^{1}H} (101 MHz) in CD_2Cl_2.

4-butyl-1-(2-hydroxy-3,5-dimethylphenyl)-3-methyl-1H-1,2,3-triazol-3-ium triflate (5a)

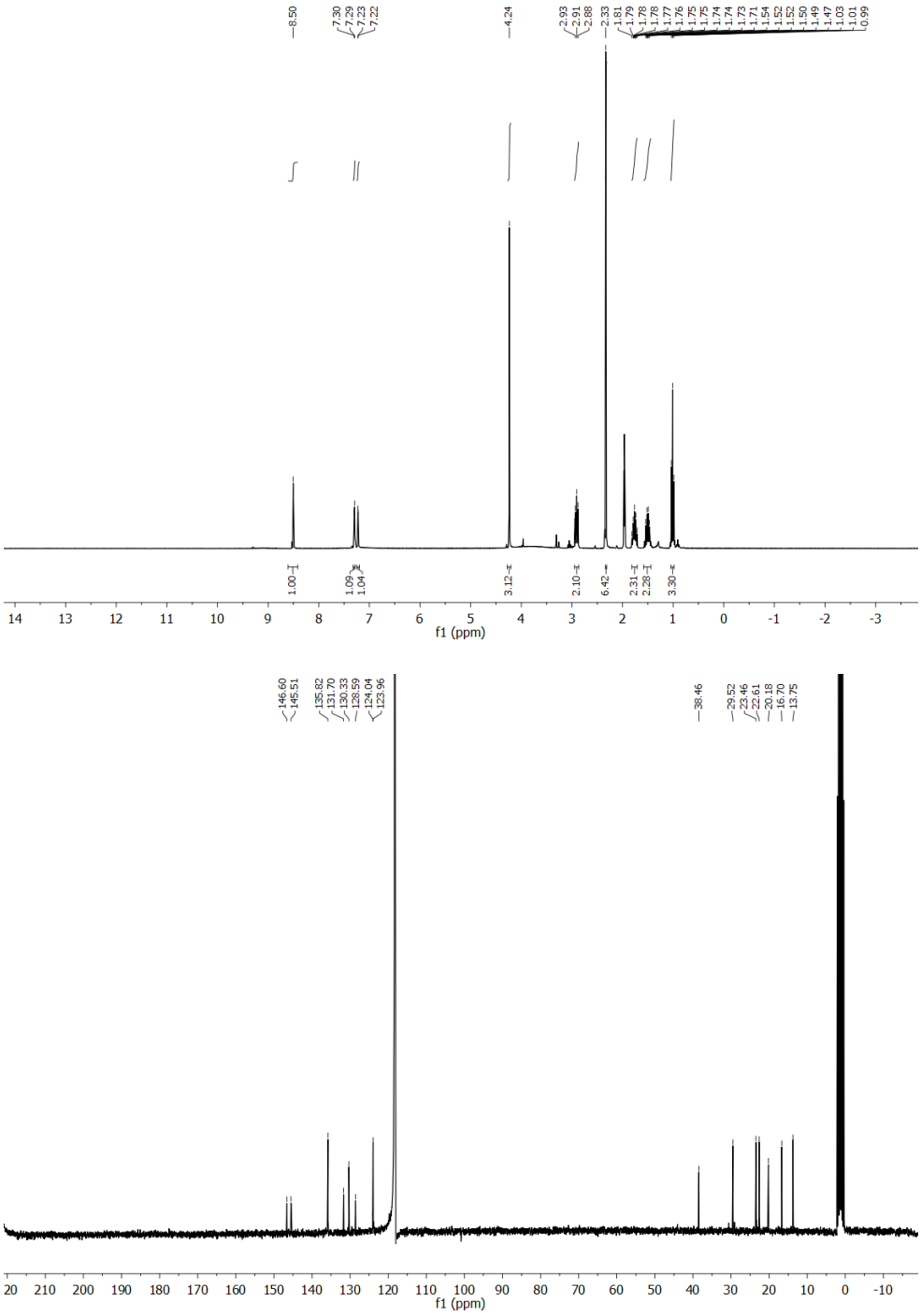

Figure S10. NMR spectra of **5a**: top ^{1}H (300 MHz), bottom $^{13}C\{^{1}H\}$ (75 MHz) in CD_3CN.

4-butyl-1-(3,5-di-tert-butyl-2-hydroxyphenyl)-3-methyl-1H-1,2,3-triazol-3-ium triflate (5b)

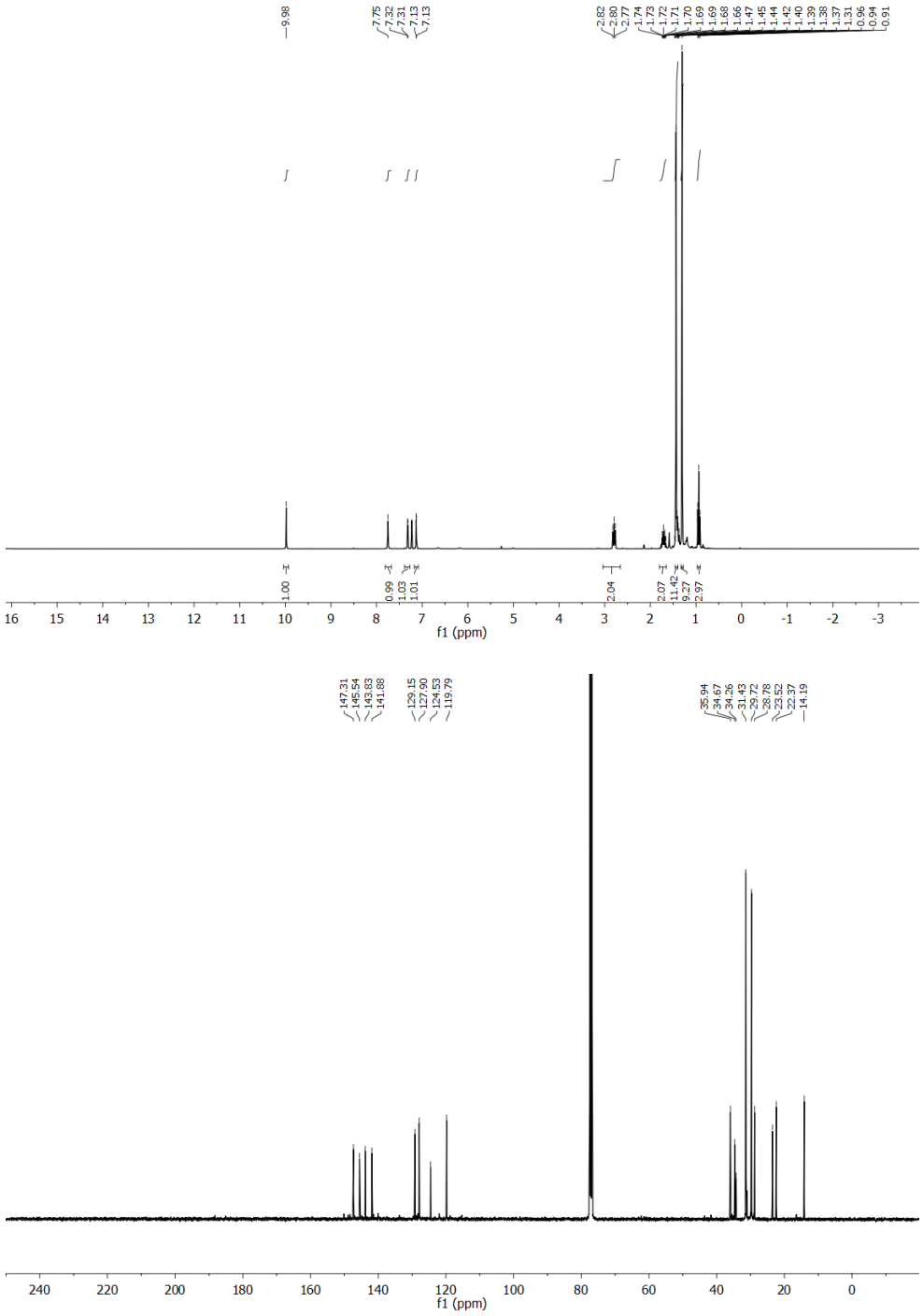

Figure S11. NMR spectra of **5b**: top ^{1}H (400 MHz), bottom $^{13}C\{^{1}H\}$ (100 MHz) in $CDCl_3$.

***cis*-[Ni(Trz^OPh(Me)$_2$)$_2$] (6a)**

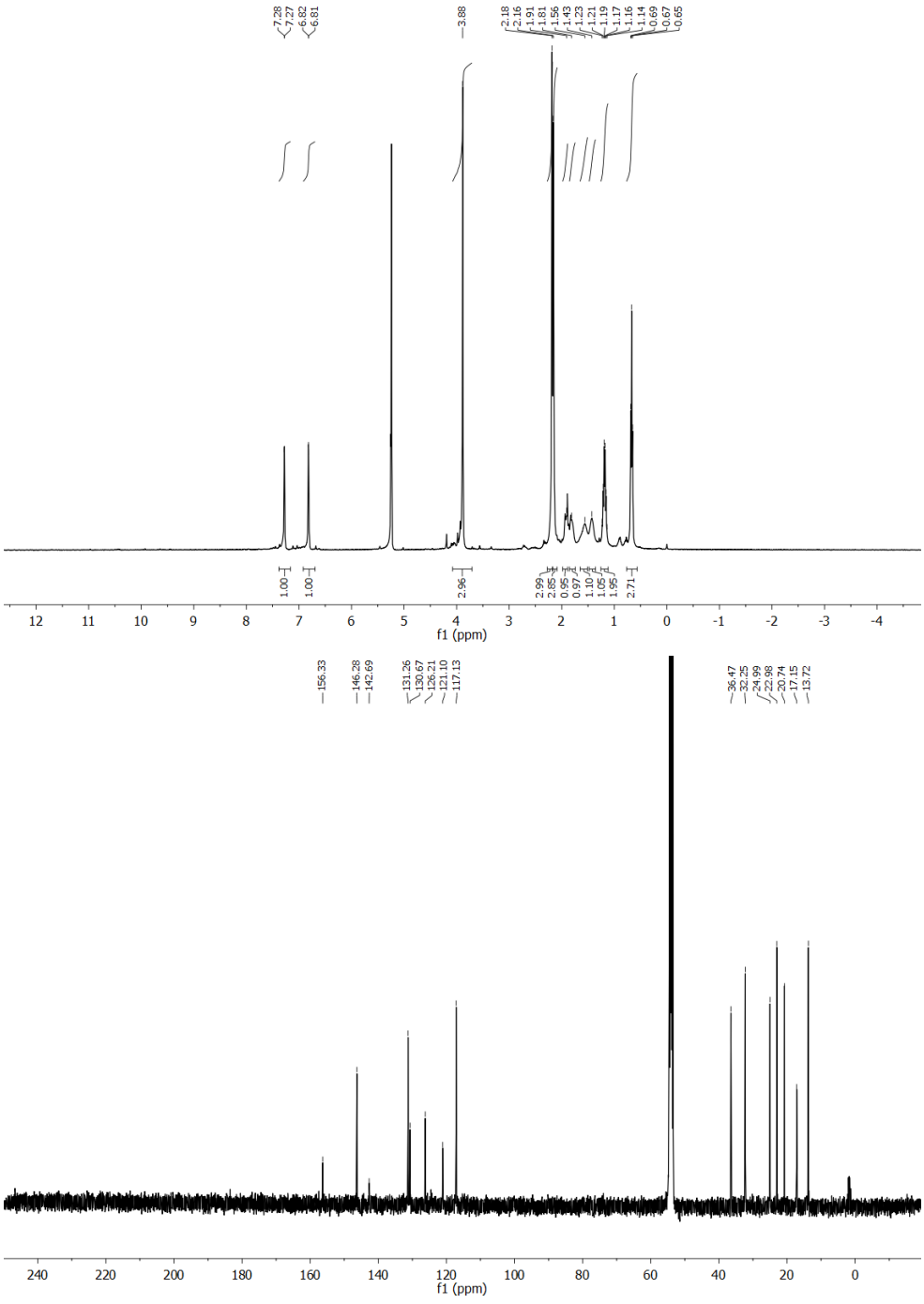

Figure S12. NMR spectra of **6a**: top ^{1}H (400 MHz), bottom ^{13}C{^{1}H} (100 MHz) in CD_2Cl_2.

***cis*-[Ni(Trz^OPh(*t*Bu)$_2$)$_2$] (6b)**

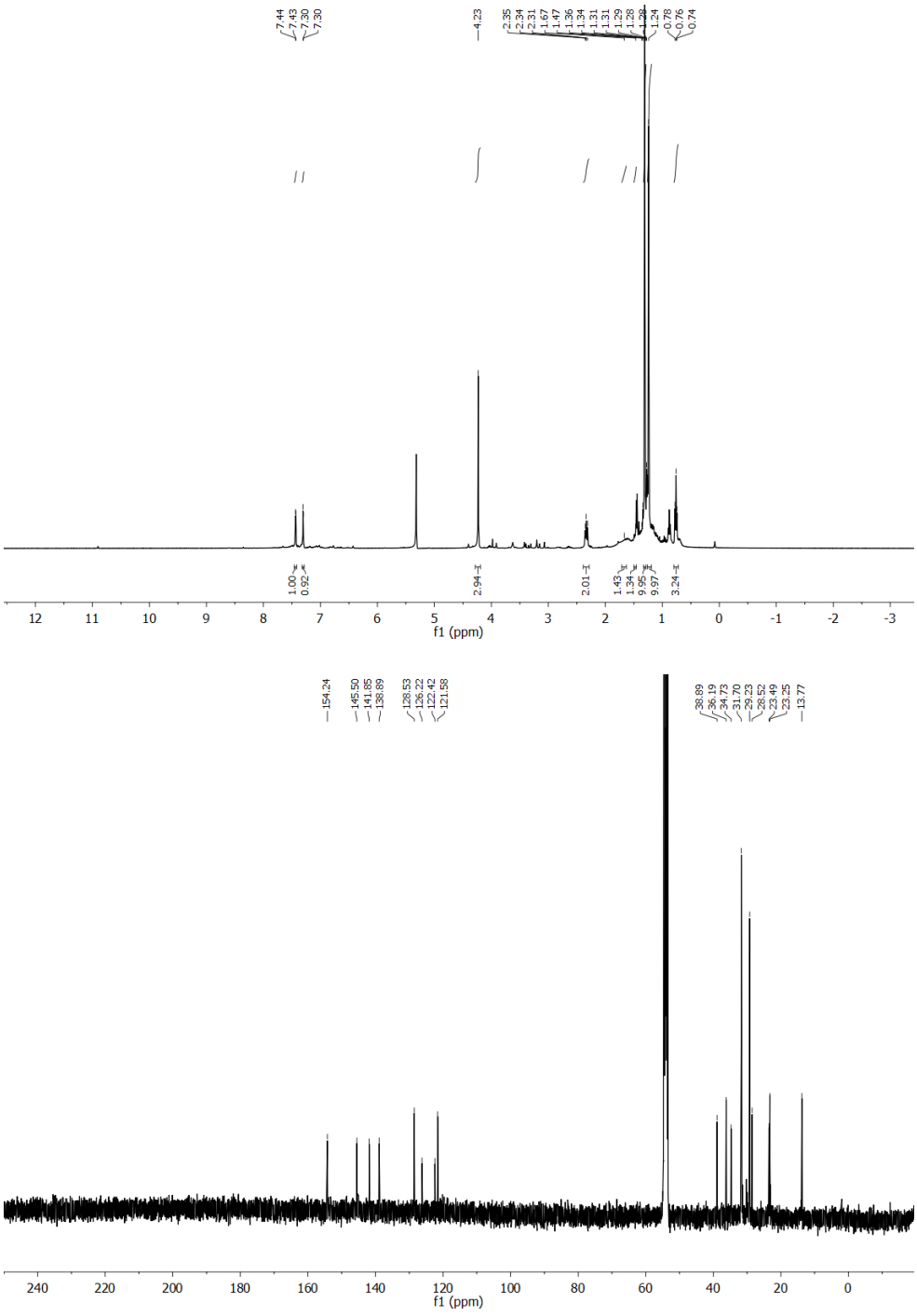

Figure S13. NMR spectra of **6b**: top ^{1}H (400 MHz), bottom ^{13}C{^{1}H} (100 MHz) in CD_2Cl_2.

1-Phenol-4-butyl-1,2,3-triazole (7a)

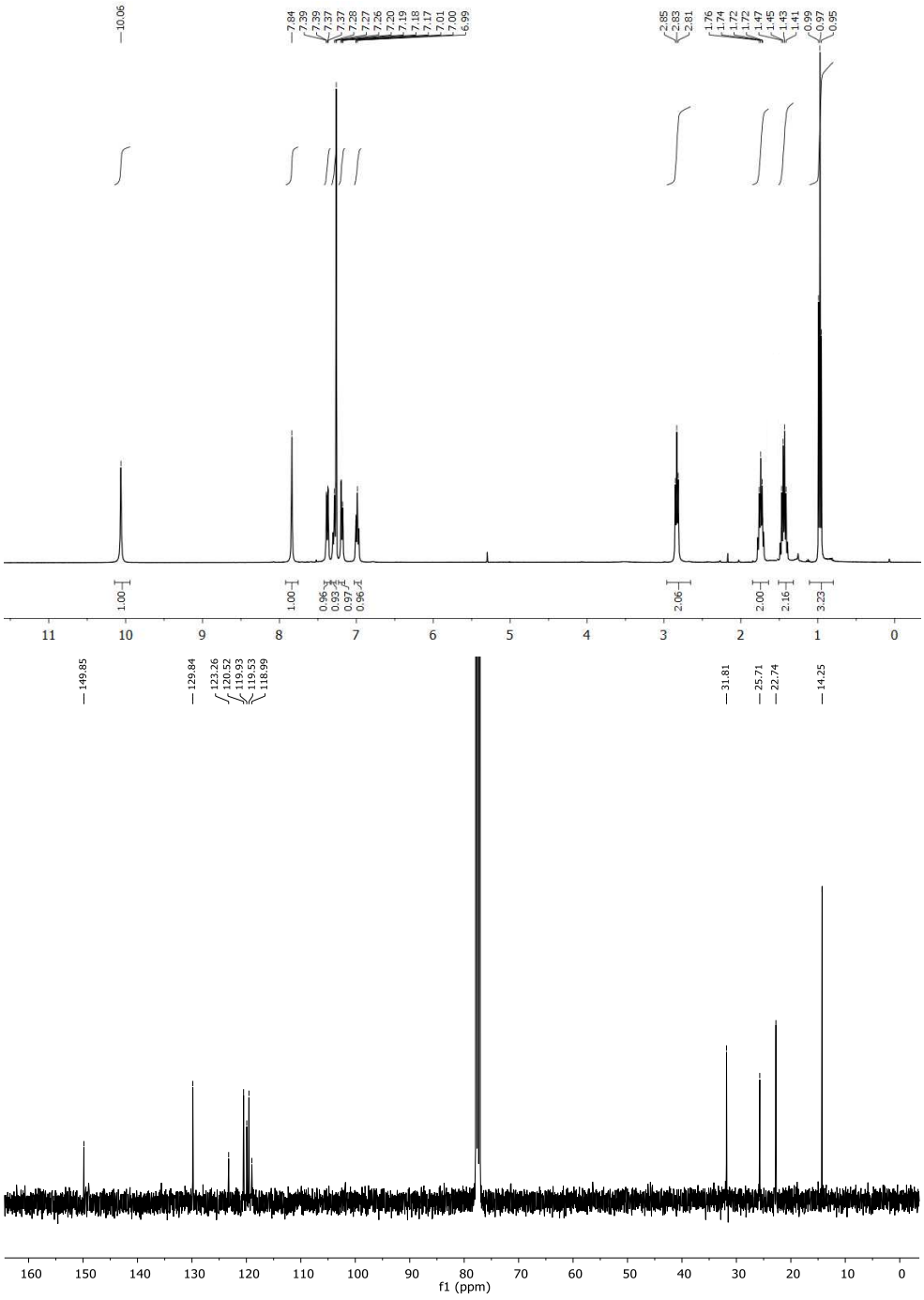

Figure S14. NMR spectra of **7a**: top ^{1}H (400 MHz), bottom $^{13}C\{^{1}H\}$ (101 MHz) in DMSO-d6.

1-Phenol-4-(2-phenyl)-1,2,3-triazole (7b)

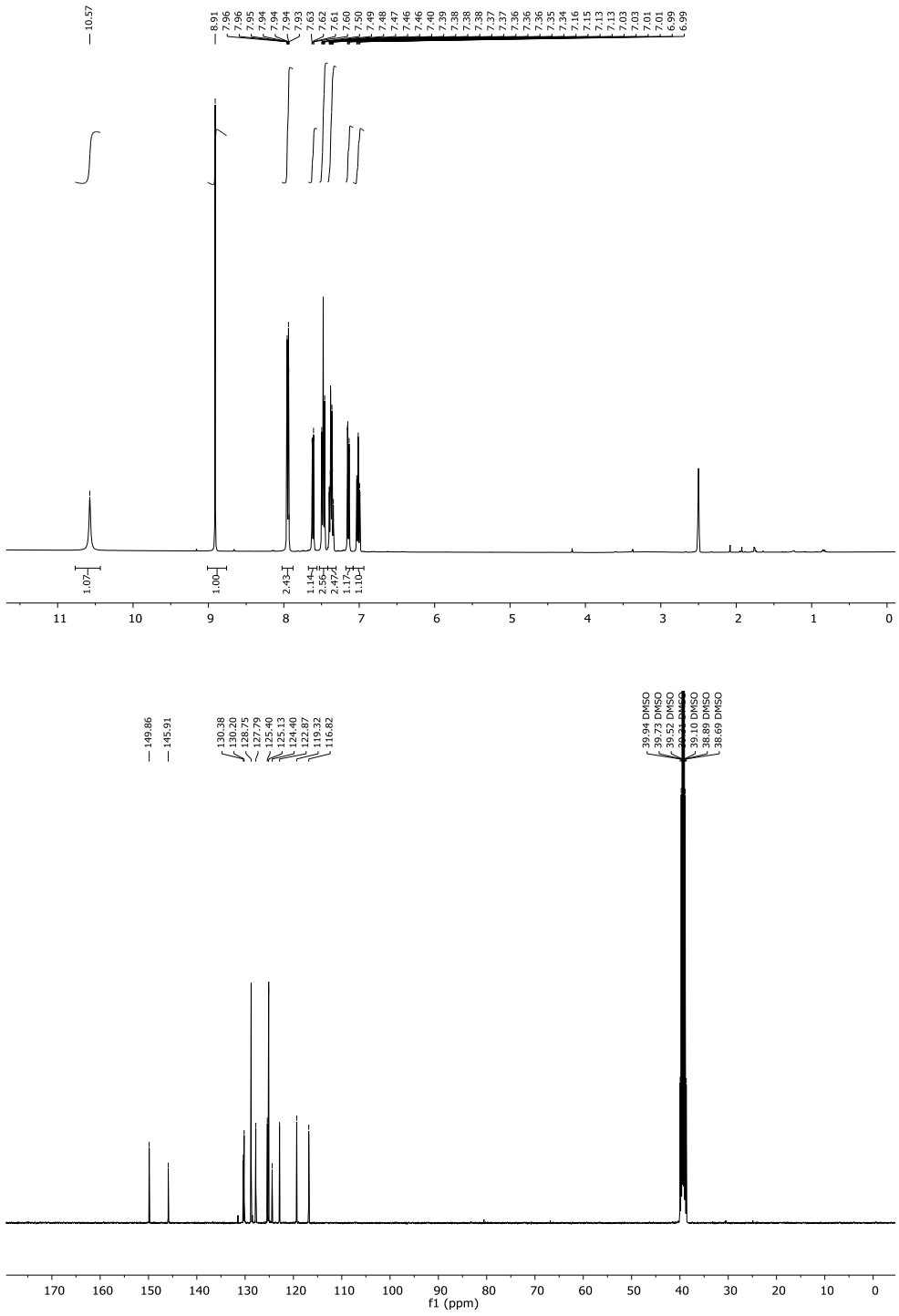

Figure S15. NMR spectra of **7b**: top ^{1}H (400 MHz), bottom $^{13}C\{^{1}H\}$ (101 MHz) in DMSO-d6.

1-Phenol-4-mesityl-1,2,3-triazole (7c)

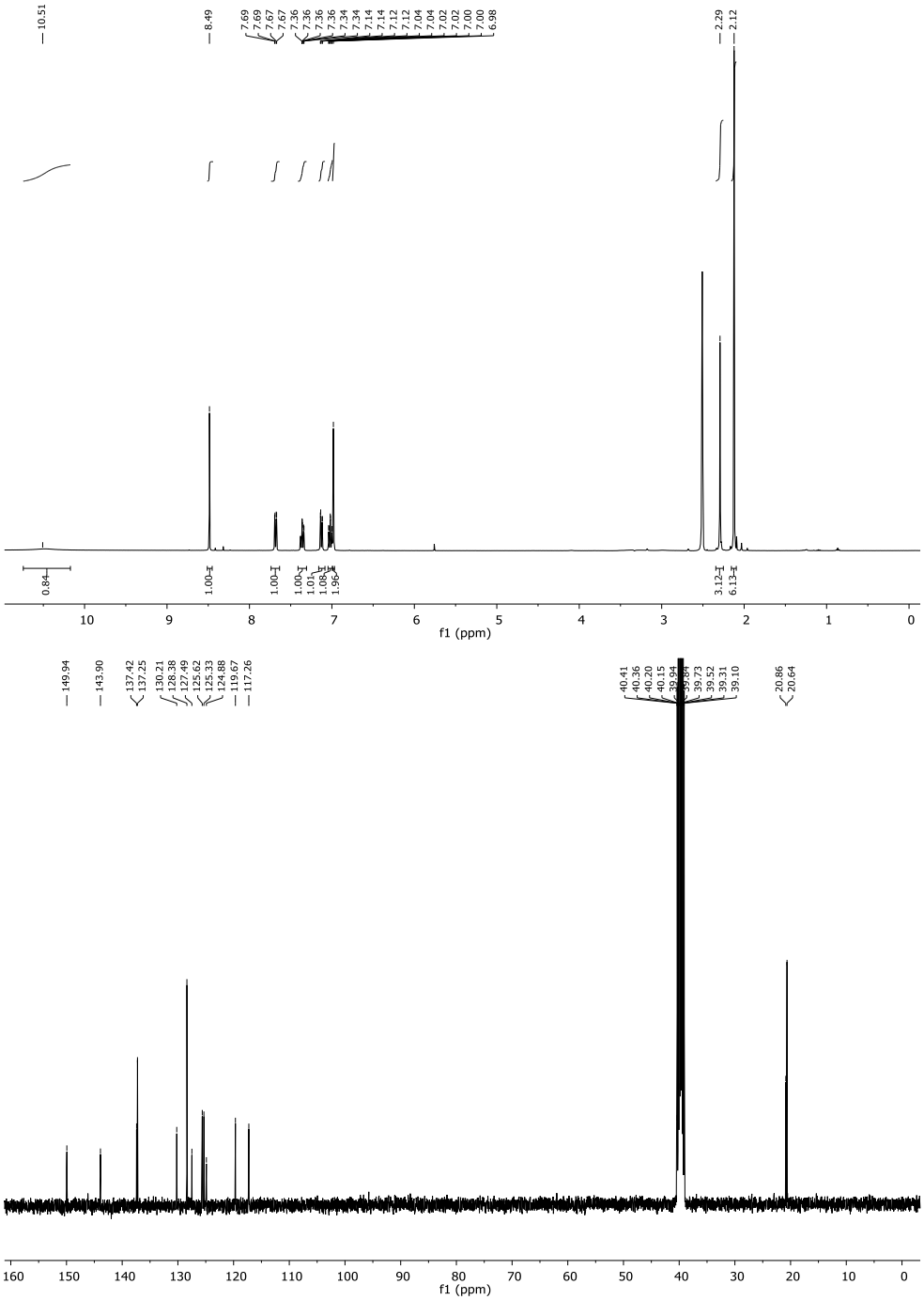

Figure S16. NMR spectra of **7c**: top ^{1}H (400 MHz), bottom $^{13}C\{^{1}H\}$ (101 MHz) in DMSO-d6.

2-(4-butyl-1H-1,2,3-triazol-1-yl)-4,6-dimethylphenol (7^{Me})

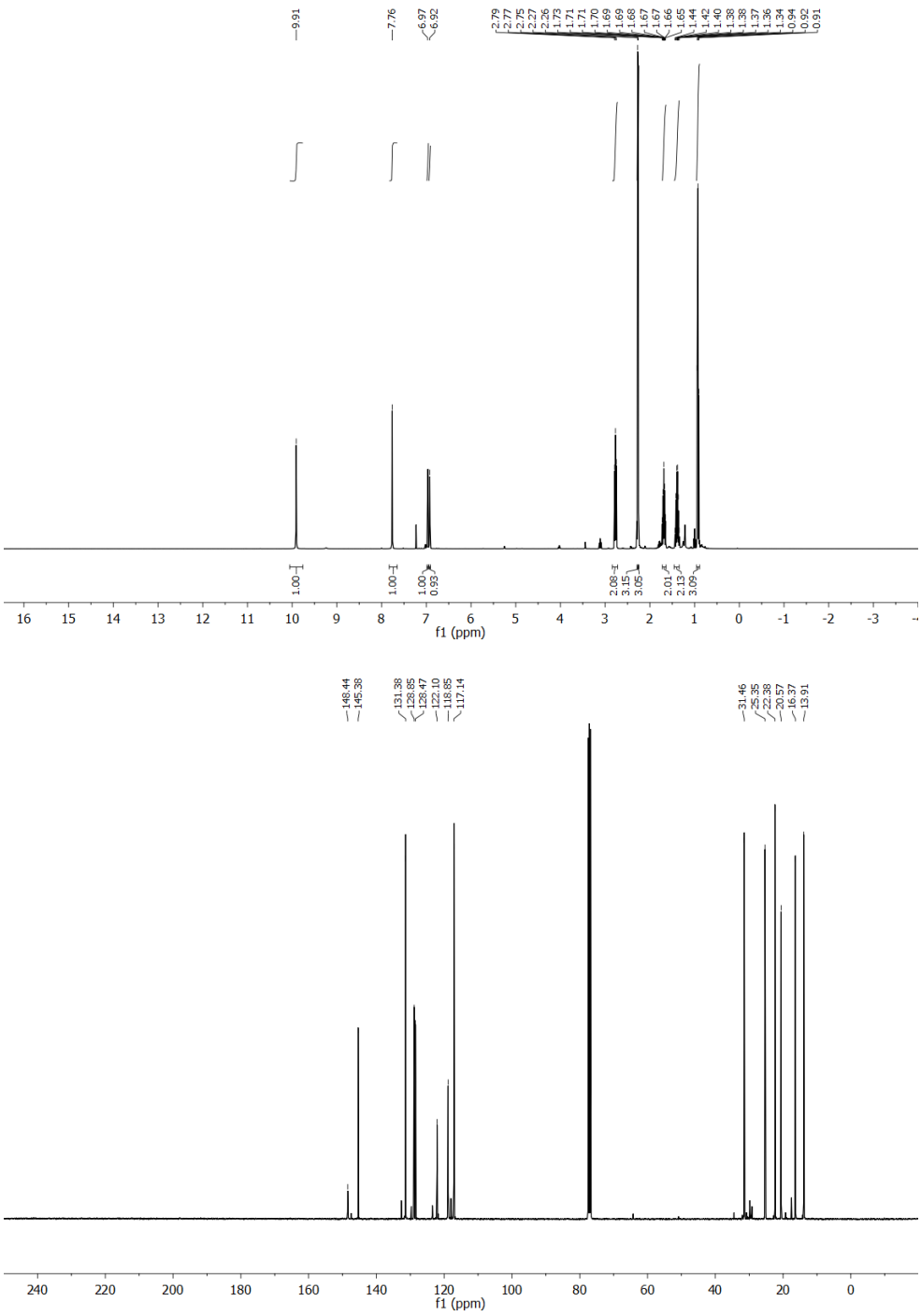

Figure S17. NMR spectra of 7^{Me}: top ^{1}H (400 MHz), bottom $^{13}C\{^{1}H\}$ (100 MHz) in $CDCl_3$.

2-(4-butyl-1H-1,2,3-triazol-1-yl)-4,6-di-tertbutylphenol (7^{tBu})

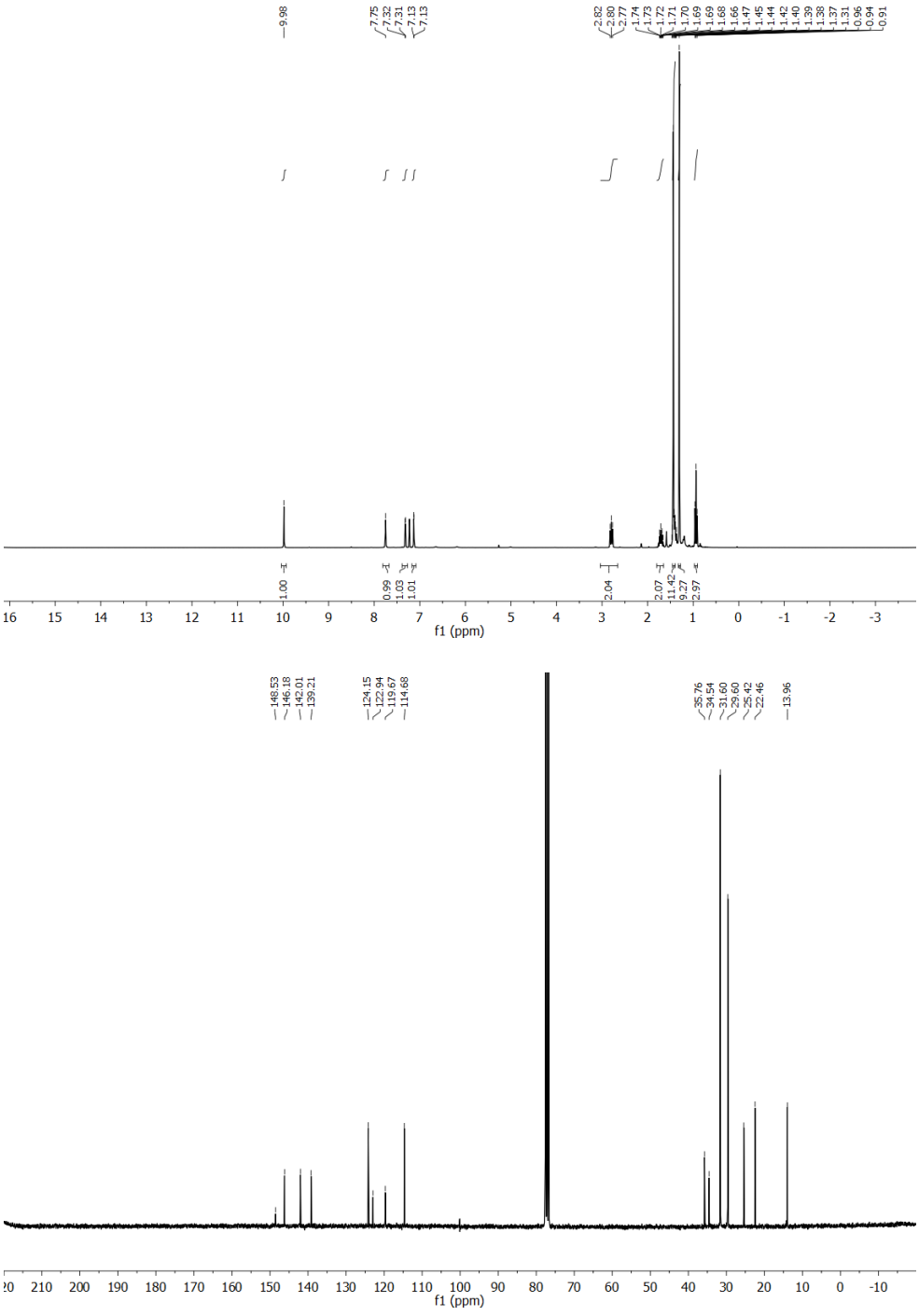

Figure S18. NMR spectra of $\mathbf{7^{tBu}}$: top ^{1}H (300 MHz), bottom $^{13}C\{^{1}H\}$ (75 MHz) in $CDCl_3$.

1-(2-phenol)-3-methyl-imidazolium iodide (9)

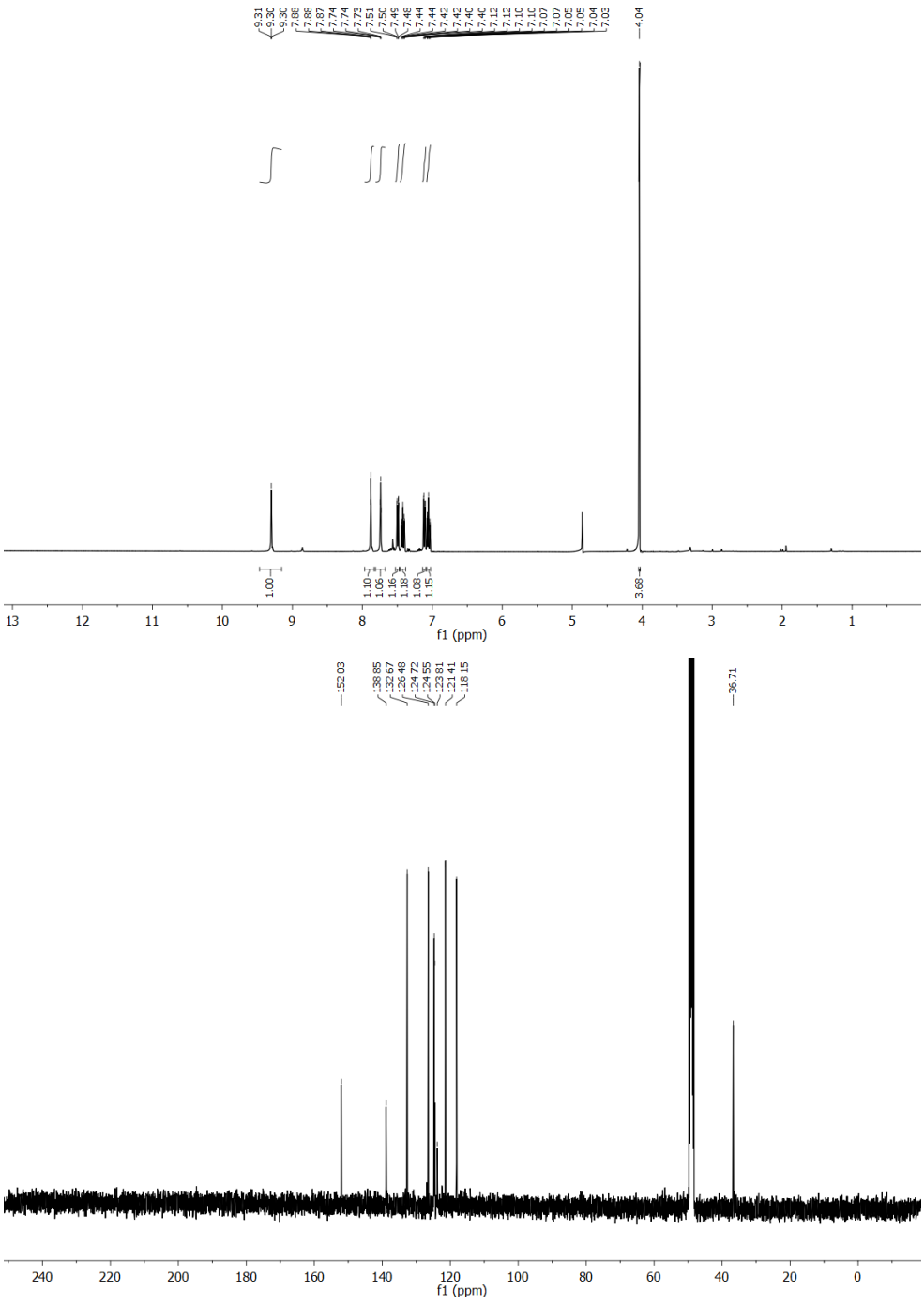

Figure S19. NMR spectra of **9**: top ^{1}H (400 MHz), bottom $^{13}C\{^{1}H\}$ (101 MHz) in CD_3OD.

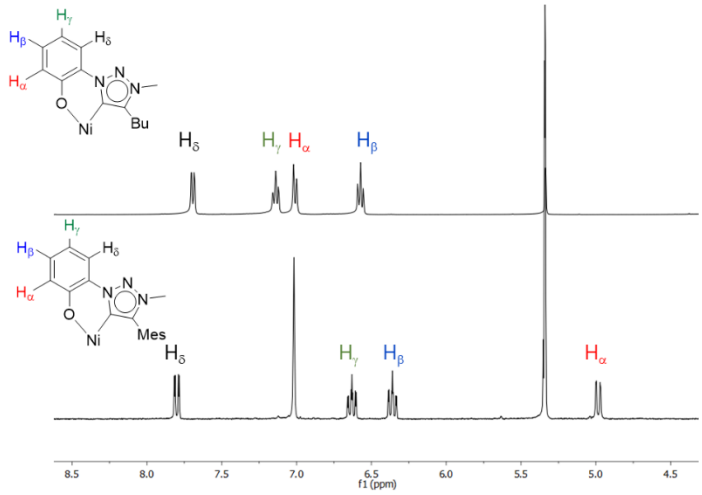

Figure S20. Comparison of the aromatic region of the ^{1}H NMR spectra of complex **3a** (top) and **3c** (bottom) revealing the substantial shift of Hα.

3. Crystal data and structure refinement for complexes 3a–c, 4, 6a–b

Crystal structure determinations

Suitable crystals of **3a–c, 4, 6a–b** were mounted in air at ambient conditions and measured on an Oxford Diffraction SuperNova area-detector diffractometer at T=173(2) K by using mirror optics monochromated $Mo_{K\alpha}$ radiation (λ=0.71073 Å) and Al filtered.[S2] Data reduction was performed by using the CrysAlisPro program.[S3] The intensities were corrected for Lorentz and polarization effects, and an absorption correction based on the multi-scan method by using SCALE3 ABSPACK in CrysAlisPro was applied. The structures were solved by direct methods by using SHELXT, and all non-hydrogen atoms were refined anisotropically.[S4]

All hydrogen atoms were placed in geometrically calculated positions and refined by using a riding model with each hydrogen atom assigned a fixed isotropic displacement parameter (1.2 Ueq of its parent atom, 1.5 Ueq for the methyl groups). Structures were refined on F^2 by using full-matrix least-squares procedures. The weighting schemes were based on counting statistics and included a factor to downweight the intense reflections. All calculations were performed by using the SHELXL-2014 program.[S5] Further crystallographic details are compiled in Tables S1–6. Crystallographic data for all structures have been deposited with the Cambridge Crystallographic Data Centre (CCDC) as supplementary publication numbers 2004183 (**3a**), 2004182 (**3b**), 2004184 (**3c**), and 2004181 (**4**), 2050371 (**6a**), 2050372 (**6b**).

Table S1. Crystal data and structure refinement for **3a**

CCDC identification code	2004183
Empirical formula	$C_{26}H_{34}N_6NiO_3$
Formula weight	537.3
Temperature/K	173(2)
Crystal system	Monoclinic
Space group	P 21/n
Unit cell dimensions	a = 12.88280(10) Å α = 90°
	b = 18.5259(2) Å β=98.7980(10)°
	c = 22.3137(3) Å γ = 90°
Volume/Å^3	5262.85(10)
Z	8
ρ_{calc}g/cm^3	1.356
μ/mm^{-1}	0.776
F(000)	2272
Crystal size/mm^3	0.384 × 0.155 × 0.008
Radiation	MoKα (λ = 0.71073)
2Θ range for data collection/°	1.72 to 28.193
Index ranges	$-16 \le h \le 16$, $-22 \le k \le 23$, $-28 \le l \le 17$
Reflections collected	32666
Independent reflections	11659 [R_{int} = 0.0288]
Data/restraints/parameters	11659/0/668
Goodness-of-fit on F^2	1.095
Final R indexes [I>=2σ (I)]	R_1 = 0.0455, wR_2 = 0.0971
Final R indexes [all data]	R_1 = 0.0623, wR_2 = 0.1047
Largest diff. peak/hole / e Å^{-3}	0.761 and –0.413

Table S2. Crystal data and structure refinement for **3b**

CCDC identification code	2004182	
Empirical formula	$C_{30}H_{24}N_6NiO_2$	
Formula weight	559.26	
Temperature/K	173(2)	
Crystal system	Monoclinic	
Space group	P 21/n	
Unit cell dimensions	a = 7.78550(10) Å	α = 90°
	b = 14.7244(2) Å	β=98.0320(10)°
	c = 22.1890(3) Å	γ = 90°
Volume/Å^3	2518.72(6)	
Z	4	
ρ_{calc}g/cm^3	1.475	
μ/mm^{-1}	0.812	
F(000)	1160	
Crystal size/mm^3	0.271 × 0.155 × 0.022	
Radiation	MoKα (λ = 0.71073)	
2Θ range for data collection/°	1.665 to 28.204	
Index ranges	$-9 \le h \le 10$, $-18 \le k \le 19$, $-28 \le l \le 28$	
Reflections collected	27724	
Independent reflections	5771 [R_{int} = 0.0376, R_{sigma} = 0.0355]	
Data/restraints/parameters	5771/0/354	
Goodness-of-fit on F^2	1.028	
Final R indexes [I>=2σ (I)]	R_1 = 0.0346, wR_2 = 0.0765	
Final R indexes [all data]	R_1 = 0.0461, wR_2 = 0.0817	
Largest diff. peak/hole / e Å^{-3}	0.323 and –0.341	

Table S3. Crystal data and structure refinement for **3c**

CCDC identification code	2004184	
Empirical formula	$C_{36}H_{36}N_6NiO_2$	
Formula weight	643.2	
Temperature/K	173(2)	
Crystal system	Monoclinic	
Space group	P 21/n	
Unit cell dimensions	a = 11.11310(10) Å	α = 90°
	b = 10.38960(10) Å	β =109.6340(10)°
	c = 14.69520(10) Å	γ = 90°
Volume/Å^3	1598.07(3)	
Z	2	
ρ_{calc}g/cm^3	1.337	
μ/mm^{-1}	0.649	
F(000)	676	
Crystal size/mm^3	0.300 x 0.250 x 0.300	
Radiation	MoKα (λ = 0.71073)	
2Θ range for data collection/°	4.014 to 54.996	
Index ranges	$-14 \le h \le 14$, $-13 \le k \le 13$, $-18 \le l \le 19$	
Reflections collected	26452	
Independent reflections	3647 [R_{int} = 0.0288]	
Data/restraints/parameters	3647/0/209	
Goodness-of-fit on F^2	1.073	
Final R indexes [I>=2σ (I)]	R_1 = 0.0298, wR_2 = 0.0817	
Final R indexes [all data]	R_1 = 0.0346, wR_2 = 0.0844	
Largest diff. peak/hole / e Å^{-3}	0.230 and –0.340	

Table S4. Crystal data and structure refinement for **4**

CCDC identification code	2004181	
Empirical formula	$C_{22}H_{20}Cl_6N_4NiO_2$	
Formula weight	643.83	
Temperature/K	173(2)	
Crystal system	Monoclinic	
Space group	I 2/a	
Unit cell dimensions	a = 15.0319(3) Å	α = 90°
	b = 11.2984(2) Å	β = 107.022(2)°
	c = 16.0579(3) Å	γ = 90°
Volume/Å^3	2607.74(9)	
Z	4	
ρ_{calc}g/cm^3	1.640	
μ/mm^{-1}	1.388	
F(000)	1304	
Crystal size/mm^3	0.532 x 0.158 x 0.071	
Radiation	MoKα (λ = 0.71073)	
2Θ range for data collection/°	2.238 to 28.150	
Index ranges	$-19 \le h \le 17$, $-14 \le k \le 14$, $-20 \le l \le 21$	
Reflections collected	11375	
Independent reflections	2948 [R_{int} = 0.0197]	
Data/restraints/parameters	2948/51/188	
Goodness-of-fit on F^2	1.052	
Final R indexes [I>=2σ (I)]	R_1 = 0.0585, wR_2 = 0.1548	
Final R indexes [all data]	R_1 = 0.0622, wR_2 = 0.1582	
Largest diff. peak/hole / e Å^{-3}	1.765 and –1.312	

Table S5. Crystal data and structure refinement for **6a**

CCDC identification code	2050371	
Empirical formula	$C_{30}H_{40}N_6NiO_2$	
Formula weight	575.39	
Temperature/K	173.01(10)	
Crystal system	Monoclinic	
Space group	*C*2/*c*	
Unit cell dimensions	a = 12.0724(2) Å	α = 90°
	b = 10.2682(2) Å	β = 102.0570(10)°
	c = 24.5315(4) Å	γ = 90°
Volume/Å^3	2973.89(9)	
Z	4	
ρ_{calc}g/cm^3	1.285	
μ/mm^{-1}	1.228	
F(000)	1224.0	
Crystal size/mm^3	0.1 × 0.05 × 0.05	
Radiation	CuKα (λ = 1.54184)	
2Θ range for data collection/°	7.37 to 154.074	
Index ranges	–15 ≤ h ≤ 13, –12 ≤ k ≤ 12, –29 ≤ l ≤ 30	
Reflections collected	14725	
Independent reflections	3073 [R_{int} = 0.0488, R_{sigma} = 0.0344]	
Data/restraints/parameters	3073/0/181	
Goodness-of-fit on F^2	1.026	
Final R indexes [I>=2σ (I)]	R_1 = 0.0448, wR_2 = 0.1225	
Final R indexes [all data]	R_1 = 0.0518, wR_2 = 0.1289	
Largest diff. peak/hole / e Å^{-3}	0.60/–0.32	

Table S6. Crystal data and structure refinement for **6b**

CCDC identification code	2050372	
Empirical formula	$C_{42}H_{64}N_6NiO_2$	
Formula weight	743.70	
Temperature/K	173.01(10)	
Crystal system	Monoclinic	
Space group	I2/a	
Unit cell dimensions	a = 12.79520(10) Å	α = 90°
	b = 18.38130(10) Å	β = 109.0670(10)°
	c = 18.97510(10) Å	γ = 90°
Volume/Å^3	4217.96(5)	
Z	4	
ρ_{calc}g/cm^3	1.171	
μ/mm^{-1}	0.970	
F(000)	1608.0	
Crystal size/mm^3	0.331 × 0.284 × 0.259	
Radiation	CuKα (λ = 1.54184)	
2Θ range for data collection/°	8.752 to 154.112	
Index ranges	$-16 \le h \le 16$, $-21 \le k \le 22$, $-23 \le l \le 23$	
Reflections collected	33030	
Independent reflections	4421 [R_{int} = 0.0252, R_{sigma} = 0.0115]	
Data/restraints/parameters	4421/75/270	
Goodness-of-fit on F^2	1.041	
Final R indexes [I>=2σ (I)]	R_1 = 0.0398, wR_2 = 0.1104	
Final R indexes [all data]	R_1 = 0.0405, wR_2 = 0.1110	
Largest diff. peak/hole / e Å^{-3}	0.42/–0.30	

Table S7. Selected bond lengths (Å), angles (deg), and τ_4 parameters for complexes **3a–c**, **4** and **6a–b**

Ni complex	**3a**	**3b**	**3c**	**4**	**6a**	**6b**
Ni–C [a)]	1.851(2)	1.8554(2)	1.924(3)	1.843(3)	1.862(2)	1.836(1)
Ni–O [a)]	1.8880(2)	1.8804(1)	1.854(2)	1.876(2)	1.887(1)	1.899(1)
O1–Ni–O2	86.02	85.88	**179.97**	86.10	85.45	89.59
C1–Ni–C2	94.86	93.67	**179.97**	94.73	94.90	92.54
C1–Ni–O1	92.12	91.88	87.64	90.48	90.58	90.40
O2–Ni–C2	90.37	91.68	87.64	90.48	90.58	90.40
C1–Ni–O2	**163.47**	**165.18**	92.36	**168.97**	**169.54**	**166.94**
O1–Ni–C2	**166.82**	**166.84**	92.36	**168.97**	**169.54**	**166.94**
τ_4 [b)]	0.21	0.20	0.00	0.15	0.15	0.18

[a)] average of Ni–C and Ni–O bonds, respectively; [b)] tetrahedral distortion parameter τ_4 calculated by $\tau_4 = [360–(\alpha+\beta)]/141$ where α and β are the two largest θ angles in the four-coordinate species according to ref S6, in the table highlighted in bold.

4. Cyclic voltammograms of complexes 3a–c, 4 and 6a–b

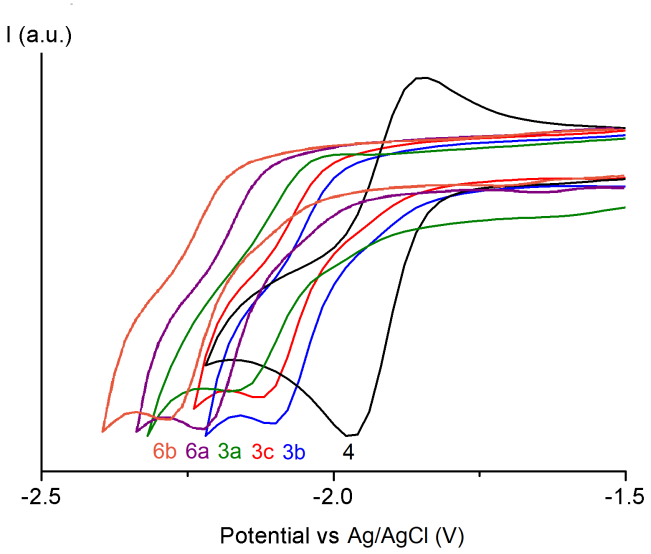

Figure S21. Cathodic section of the cyclic voltammograms of Ni(II) complexes **3a–c**, **4**, **6a–b** (1 mM in MeCN with 0.1 M $(Bu_4N)PF_6$ as supporting electrolyte, 100 mV s^{-1} scan rate, Fc^+/Fc as internal standard with $E_{1/2}$ = 0.36 V *vs* Ag/AgCl.

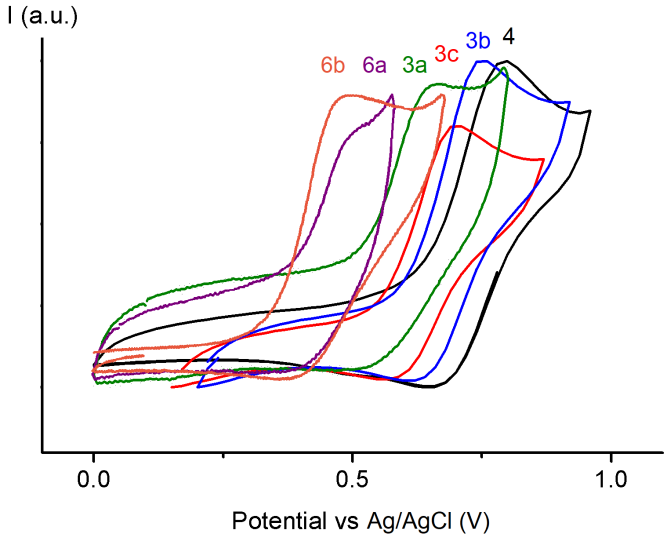

Figure S22. Anodic section of the cyclic voltammograms of Ni(II) complexes **3a–c**, **4**, **6a–b** (1 mM in MeCN, 0.1 M with 0.1 M $(Bu_4N)PF_6$ as supporting electrolyte, 100 mV s^{-1} scan rate, Fc^+/Fc as internal standard with $E_{1/2}$ = 0.36 V *vs* Ag/AgCl).

5. NMR and CV experiments in acidic media with complex 3a

The instability of the catalytic current in proton reduction has been attributed to a low stability of the Ni species in acidic solution, since CV measurements of the Ni complex **3a** in the presence of 2 eq. triflic acid (TFA) afforded a new species that displays an irreversible reduction at higher potential than **3a** and no oxidation up to 0.8 V (Fig. S15). Formation of a new species upon protonation was also supported by ^{1}H NMR spectroscopy. Complex **3a** gradually degrades in the presence of acetic acid (CD_3COOH) quantitatively to the triazolium salt as a consequence of carbene protonation (CD_3CN solution, Fig. S16). This degradation is slow in the presence of 2 eq. acid (days), yet much faster when larger excess of acid is used (few hours with 20 equiv). This acid lability therefore requires a flow process with a steady yet low proton supply for high turnover proton reduction with these nickel complexes.

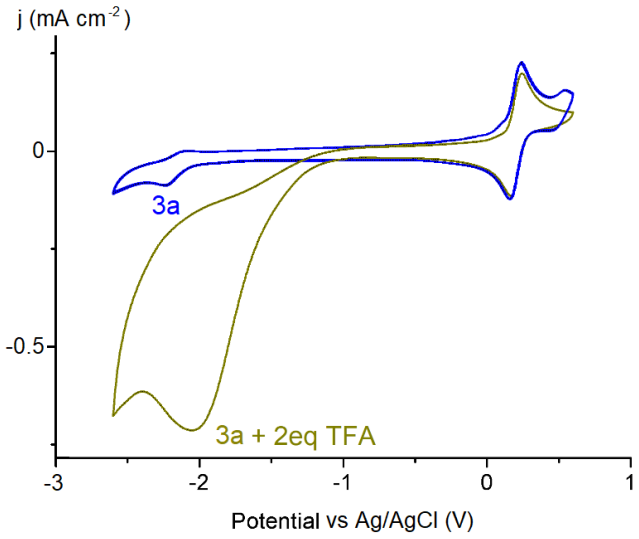

Figure S23. CV measurements of complex **3a** with triflic acid (TFA 2 mM; green line) and without TFA (blue line). Measurements with **3a** (1 mM) in MeCN with $(Bu_4N)PF_6$ (0.1 M) as supporting electrolyte, scan rate 250 mV s^{-1}; Fc^+/Fc as internal standard with $E_{1/2}$ = 0.36 V *vs* Ag/AgCl.

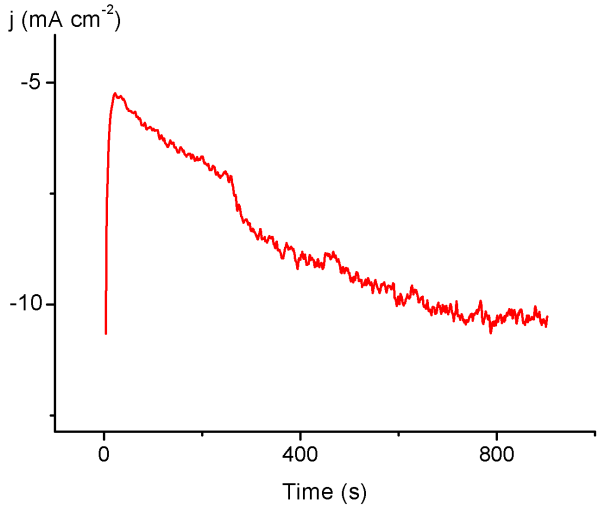

Figure S24. Electrolysis experiment performed with 1 mM complex **3a,** at –1.7 V *vs* Ag/AgCl, with acetic acid (AcOH, 100 mM) using glassy carbon working electrode, in MeCN with $(Bu_4N)PF_6$ (0.1 M) as supporting electrolyte.

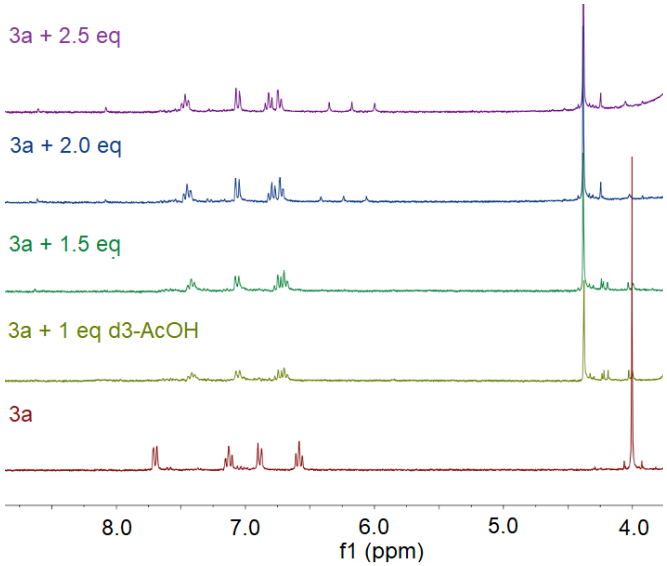

Figure S25. ^{1}H NMR spectra of complex **3a** in CD_3CN (300 MHz, 298 K) with increasing amounts of CD_3COOH (0, 1, 1.5, 2, and 2.5 eq, respectively).

6. Electrochemical set-up and product quantification

Cyclic voltammograms for the electrochemical characterization of the complexes were recorded using a Metrohm Autolab Model PGSTAT101 potentiostat employing a gas-tight three-electrode compartment cell under an Ar or a CO_2 atmosphere. The MeCN solutions (10 mL solvent, 1 mM sample, and 100 mM $(Bu_4N)PF_6$ as supporting electrolyte) were deaerated by bubbling with Ar (99.9999%, Carbagas, Switzerland) for 15 min prior to each run. When required the solutions were saturated by bubbling CO_2 (99.9999%, Carbagas, Switzerland) for 30 min under continuous stirring. The electrolysis experiments were carried out using a potentiostat/galvanostat Metrohm Autolab 128N. The CO_2 reduction was carried out at room temperature using a custom-made H-type glass cell where a proton exchange membrane (Nafion 21, Fuel Cell Store, 50.8 µm thickness, weight: 100 g m^{-2}) was used to separate cathode and anode compartment of the electrochemical cell. All potentials were measured using a glassy carbon (GC-rod, 7.0 mm^2 or GC-foil, 112 mm^2) working electrode, a Ag/AgCl (saturated KCl) reference electrode and a Pt wire auxiliary electrode and are tabulated versus a ferrocene internal standard. The Fc^+/Fc couple is 0.36 V *vs* Ag/AgCl in 0.1 M $(Bu_4N)PF_6$ MeCN solutions.[S7]

The apparent rates (k_{obs}) were determined directly from voltammograms of active catalysts.[S6] The model analyses CV responses for the reduction of substrate A to B by a redox catalyst P, where the rate-limiting step is homogeneous electron transfer (the E_rC_i' mechanism).[S8] The theory behind the CV of catalytic E_rC_i' reactions was formulated by Delahay and Stiehl,[S9] Nicholson and Shain,[S10, S11] and Savéant and co-workers.[S10–S14] The resulting current wave can be described by the following equation:

$$i = \frac{nFAC_P^0\sqrt{Dk_{obs}}}{1 + \exp\left[\frac{nF}{RT}(E - E_{P/Q}^\circ)\right]}$$

where, n is the number of electrons transferred in the redox event, A the electrode surface area in cm^2, D the diffusion coefficient of the redox species P in $cm^2\ s^{-1}$, and C_P^0 the bulk concentration of redox species P in mol cm^{-3}. The i–k_{obs} relationship is divided by the Randles−Sevcik equation, which describes the dependence of the peak current i_p (amperes) on the scan rate υ (V s^{-1}), yielding to the following relationship.[S10]

$$\frac{i_c}{i_P} = \frac{1}{0.446}\sqrt{\left(\frac{RT}{nF\upsilon}\right)k_{obs}}$$

where i_c is the catalytic current peak, i_p is the current peak in absence of catalyst and F = 96485.33 C mol^{-1} and R= 8.31446 $J \cdot K^{-1} \cdot mol^{-1}$. Values used for the determination of the k_{obs} are provided below in Tables S8 and S9.

Table S8. i_c/i_p values used for k_{obs} determination in electrocatalytic H^+ reduction [a)]

Ni complex	i_c/i_p	k_{obs} (s^{-1}) [b)]
3a	10.66	440
3b	8.80	300
3c	1.60	10
4	7.81	200

[a)] general conditions; 1 mM MeCN solution of Ni complex with AcOH (0.8 M), $(Bu_4N)PF_6$ as supporting electrolyte, 250 mV s^{-1} scan rate, Fc^+/Fc as internal standard with $E_{1/2}$ = 0.36 V *vs* Ag/AgCl. k_{obs} calculated at p = 1 atm, T = 25 ºC, and for n = 2. [b)] determined from foot of the wave data treatment.

Table S9. i_c/i_p values used for k_{obs} determination in electrocatalytic CO_2 reduction [a)]

Ni complex	i_c/i_p
3a	8.50
3b	7.53
3c	1.57
4	6.22
6a	9.11
6b	11.23

[a)] general conditions: 1mM MeCN of Ni complex saturated with CO_2, $(Bu_4N)PF_6$ as supporting electrolyte, 250 mV s^{-1} scan rate, Fc^+/Fc as internal standard with $E_{1/2}$ = 0.36 V *vs* Ag/AgCl. k_{obs} calculated at p = 1 atm, r.t., and for n = 2.

Product analysis by gas chromatography: A gas chromatograph (GC 8610C device, SRI Instruments, USA), equipped with a packed Hayesep D column and a packed Molesieve 5A column, was used to carry out the product quantification. Argon (99.9999 %, Carba Gas, Switzerland) was used as a carrier gas. During the CO_2 electrolysis, the catholyte was continuously purged with CO_2 at a constant flow rate of 10 mL min^{-1}. The headspace of cathode compartment of the H-type cell was directly connected to the gas sampling loop of the GC. CO quantification was carried out with a flame ionization detector (FID) assembled with a methanizer. H_2 (formed as a side product) was quantified by a thermal conductivity detector (TCD). The following equation was used to calculate the individual partial current (I_i) of each gaseous product formed during the electrochemical CO_2 reduction

$$I_i = \frac{c_i \cdot v \cdot F \cdot z}{10^6 \cdot V_m}$$

where I_i defines the partial current for a certain product i, z the number of electrons transferred, c_i the amount of product obtained in ppm, F the Faraday constant in C/mol, v is the flow rate in L/s and V_m the molar volume of gas at 1 atm and RT in L/mol. By dividing the individual partial current with the total electrolysis current (I_{total}), the Faradaic efficiency (FE) of a certain gaseous product was obtained.

$$FE = \frac{I_i}{I_{total}} \cdot 100\%$$

Quantification of non-volatile liquid products (e.g. formate), accumulated in the catholyte during the CO_2 electroreduction, was carried out by means of ion exchange chromatography (IC, Metrohm Advanced Modular Ion Chromatograph: L-7100 pump, Metrosep A Supp 7-250 column). A conductivity detector was used for liquid product quantification. The corresponding partial charge was calculated and then it was divided by the total charge (transferred throughout the entire electrolysis experiment) to obtain the Faradaic efficiency.

$$Q_i = \frac{V_{cath} \cdot F \cdot z}{10^3 \cdot M} \cdot c_i$$

$$FE = \frac{Q_i}{Q_{total}} \cdot 100\%$$

where Q_i is the partial charge involved for the formation of an individual product i (here formate), V_{cath} is the whole volume of the catholyte in L, C_i is the amount of the product i in ppm, M is the molar mass, F is the Faraday constant and z is the number of electron transferred to form the product from CO_2. The total charge transferred during the electrolysis experiment is denoted as Q_{total}.

Table S10. Faradaic efficiencies (FE) for formate, catalytic rates, and selectivity for complexes **3a–c** and **4** for the electrochemical reduction of CO_2 [a)]

Ni complex	*FE* /%				k_{obs} (s^{-1}) [b)]
	2 h	4 h	8 h	24 h	
3a	45	54	68	70	280
3b	37	43	47	47	220
3c	9	10	10	10	10
4	22	25	25	25	150
6a	54	70	74	74	300
6b	70	82	83	83	370

[a)] general conditions: potentiostatic CO_2 electroreduction experiments performed with 1 mM complex, at –1.9 V *vs* Ag/AgCl, using glassy carbon working electrode and a Pt foil as counter electrode in a solution of MeOH/MeCN 1:50 v:v with 0.1 M $(Bu_4N)PF_6$ as supporting electrolyte [b)] determined from foot of the wave data treatment.

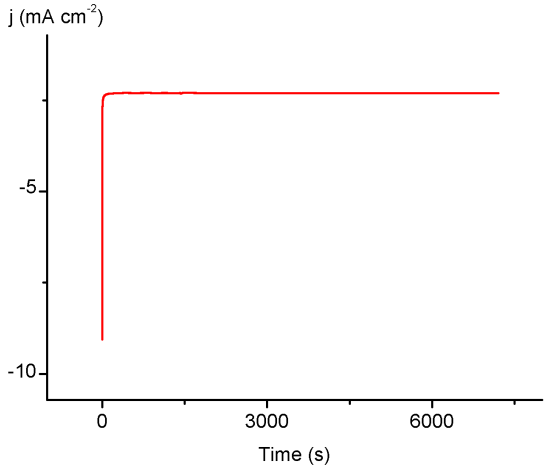

Figure S26. Electrolysis experiment performed with 1 mM complex **3a**, at –1.9 V *vs* Ag/AgCl, using glassy carbon working electrode, in a CO_2 saturated solution of MeOH/MeCN 1:50 v:v with 0.1 M $(Bu_4N)PF_6$ as supporting electrolyte.

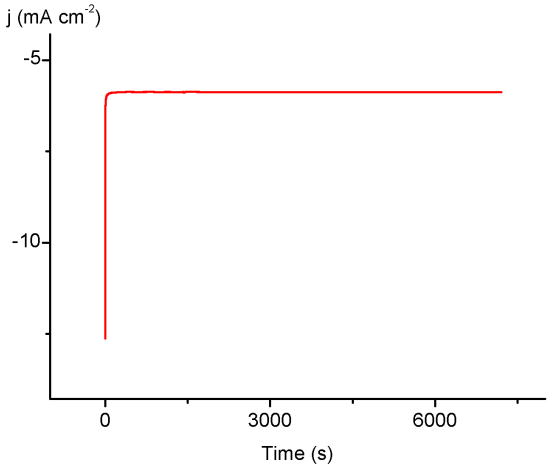

Figure S27. Electrolysis experiment performed with 1 mM complex **3b**, at –1.9 V *vs* Ag/AgCl, using glassy carbon working electrode, in a CO_2 saturated solution of MeOH/MeCN 1:50 v:v with 0.1 M $(Bu_4N)PF_6$ as supporting electrolyte.

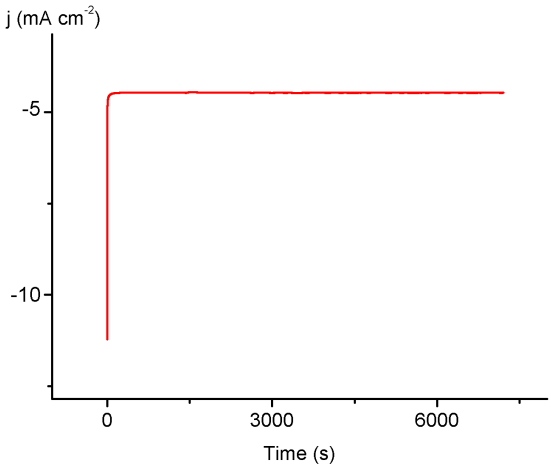

Figure S28. Electrolysis experiment performed with 1 mM complex **3c**, at –1.9 V *vs* Ag/AgCl, using glassy carbon working electrode, in a CO_2 saturated solution of MeOH/MeCN 1:50 v:v with 0.1 M $(Bu_4N)PF_6$ as supporting electrolyte.

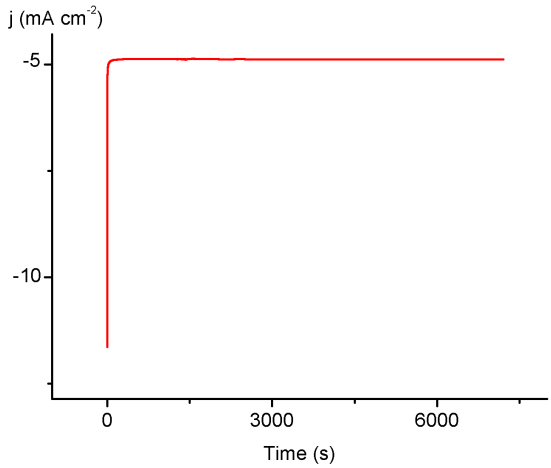

Figure S29. Electrolysis experiment performed with 1 mM complex **4**, at –1.9 V *vs* Ag/AgCl, using glassy carbon working electrode, in a CO_2 saturated solution of MeOH/MeCN 1:50 v:v with 0.1 M $(Bu_4N)PF_6$ as supporting electrolyte.

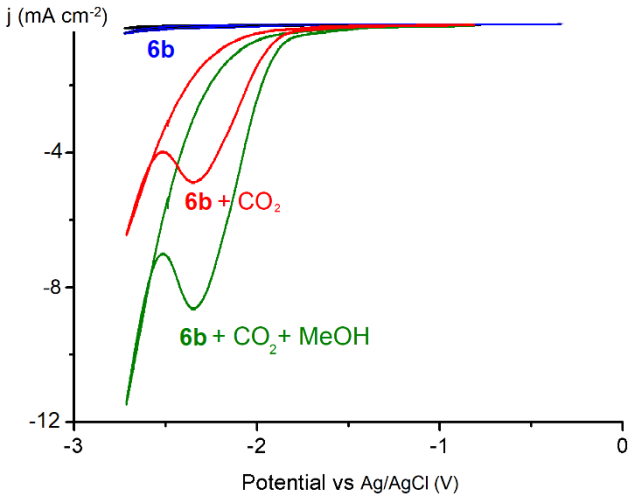

Figure S30. Catalytical electroreduction of CO_2 in MeCN with complex **6b** (0.1 M $(Bu_4N)PF_6$ as supporting electrolyte, 250 mV s^{-1} scan rate, glassy carbon working electrode); black line: CO_2-saturated MeCN solution; blue line: degassed solution of complex **6b** (1 mM) under Ar; red line: complex **6b** (1 mM) in CO_2-saturated MeCN solution; green line: complex **6b** (1 mM) in CO_2-saturated MeCN solution with 40 eq MeOH).

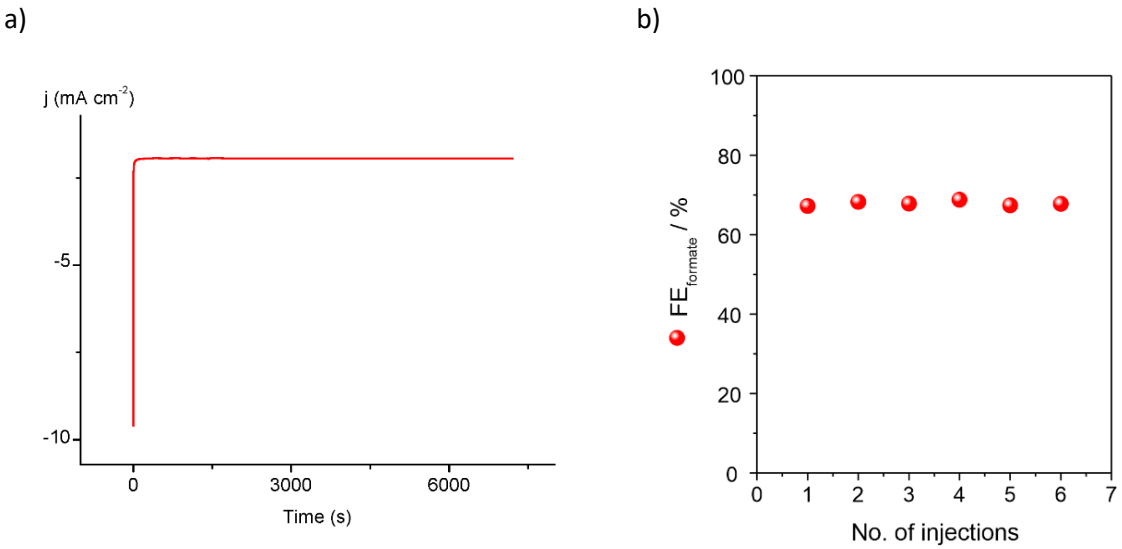

Figure S31. a) Electrolysis experiment performed with 1 mM complex **6a**, at –1.9 V *vs* Ag/AgCl, using glassy carbon working electrode, in a CO_2 saturated solution of MeOH/MeCN 1:50 v:v with 0.1 M $(Bu_4N)PF_6$ as supporting electrolyte. b) Faradaic efficiencies obtained by electrolysis experiment performed with 1 mM complex **6b**, at –1.9 V *vs* Ag/AgCl, using glassy carbon working electrode, in a CO_2 saturated solution of MeOH/MeCN 1:50 v:v with 0.1 M $(Bu_4N)PF_6$ as supporting electrolyte (see also Fig. 6 main text). The product was quantified by IC and the analysis was repeated on 6 different injections after 2h of electrolysis.

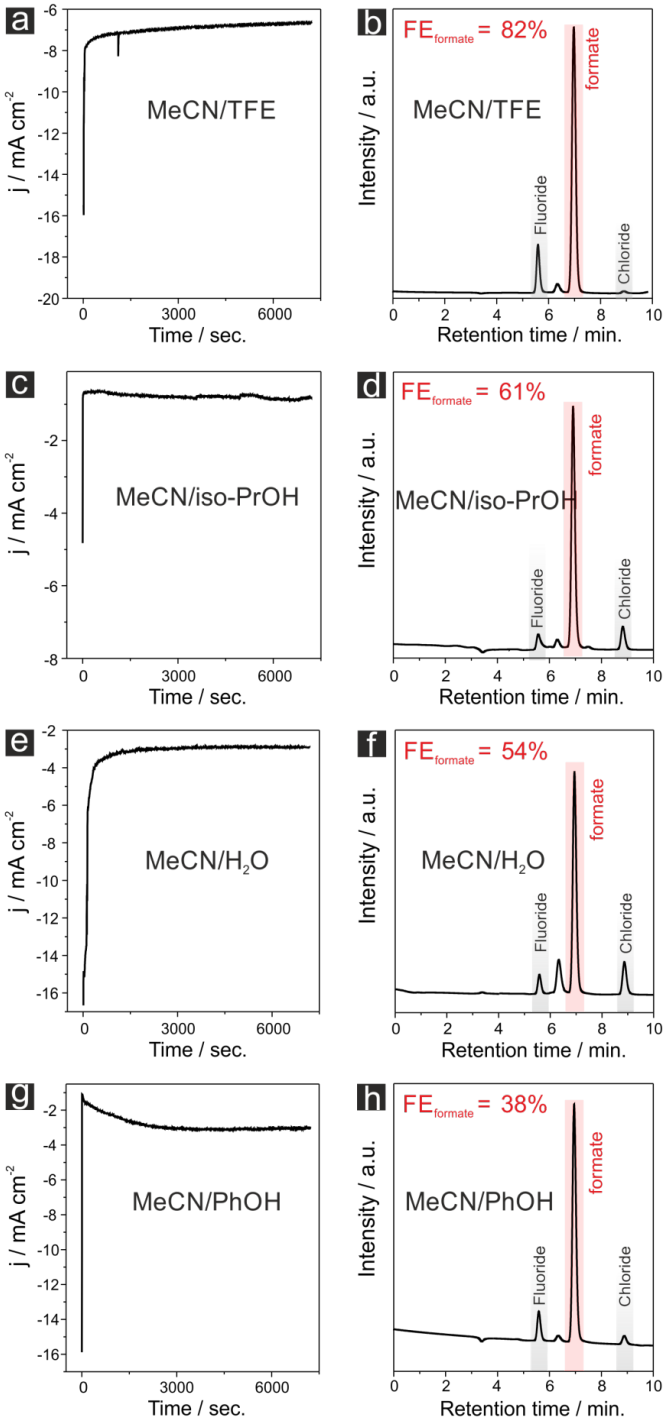

Figure S32. Current transients (*current density* vs. *electrolysis time* plots) of the potentiostatic CO_2 reduction at -1.9 V *vs* Ag/AgCl using glassy carbon working electrode, in a CO_2 saturated MeCN solution, containing 1 mM complex **6b**, 0.5 M of the proton donor and 0.1 M $(Bu_4N)PF_6$ as supporting electrolyte (panels a, c, e, and g), and corresponding post-electrolysis ion chromatograms (panels b, d, f, and h). The resulting faradaic efficiencies for formate are indicated in the respective chromatogram. The applied potential has been *iR*-corrected (79-82% of the cell resistance); the *iR* drop has been determined prior to the electrolysis for each individual measurement by means of the positive feedback method.

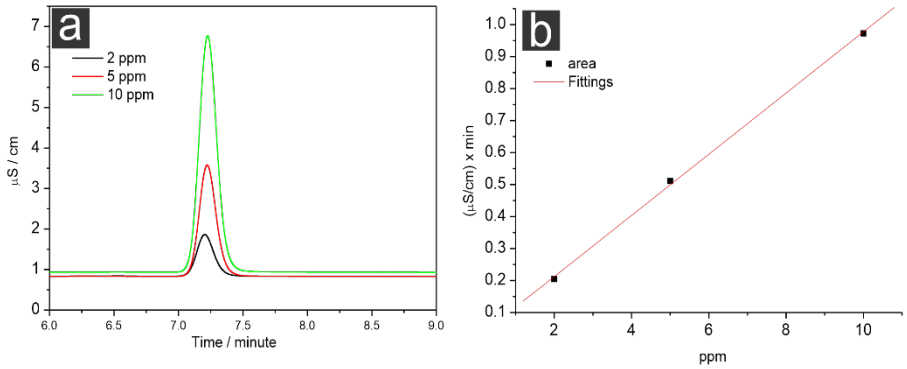

c

Formate conc (ppm)	Retention time (minute)	Height (µS/cm)	Area, (µS/cm)x min
2	7.31	1.257	0.205
5	7.32	3.140	0.511
10	7.32	5.911	0.973

Figure S33. (a) Chromatograms of standard formate reference samples used for calibration purposes. Chromatograms were measured from 2, 5, and 10 ppm formate samples, prepared from a 1000 ppm IC standard solution, procured from Sigma Aldrich. (b) Area *vs* concentration calibration curve was obtained from the measurements of the standard samples; (c) Table showing the results in terms of formate retention times, peak heights and peak areas for the three different standard samples (adopted from ref. S16).

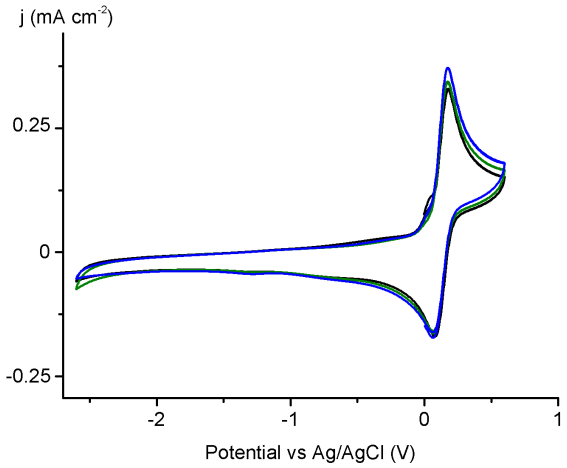

Figure S34. Control experiments using 1mM Fc as i.s. and 0.1 M $(Bu_4N)PF_6$ as supporting electrolyte: CV of a solution of MeOH/MeCN 1:50 v:v (black line), CV of a CO_2 saturated solution of MeOH/MeCN 1:50 v:v (green line) and CV of the same CO_2 saturated solution of MeOH/MeCN 1:50 v:v after purging N_2 for 30 mins (blue line).

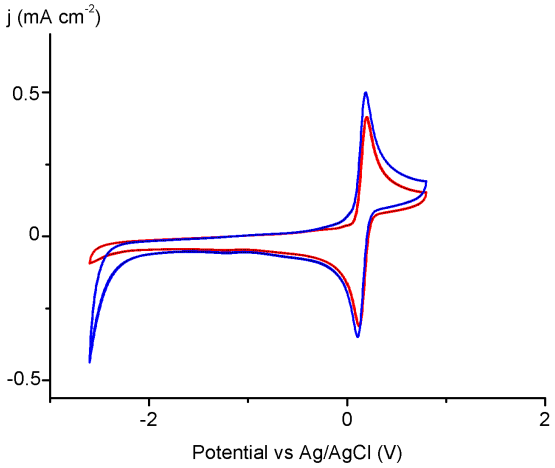

Figure S35. Control experiments using 1mM Fc as internal standard and 0.1 M $(Bu_4N)PF_6$ as supporting electrolyte: CV of a pure MeCN solution (red line) and CV of a 5 mM acetic acid in MeCN solution (blue line).

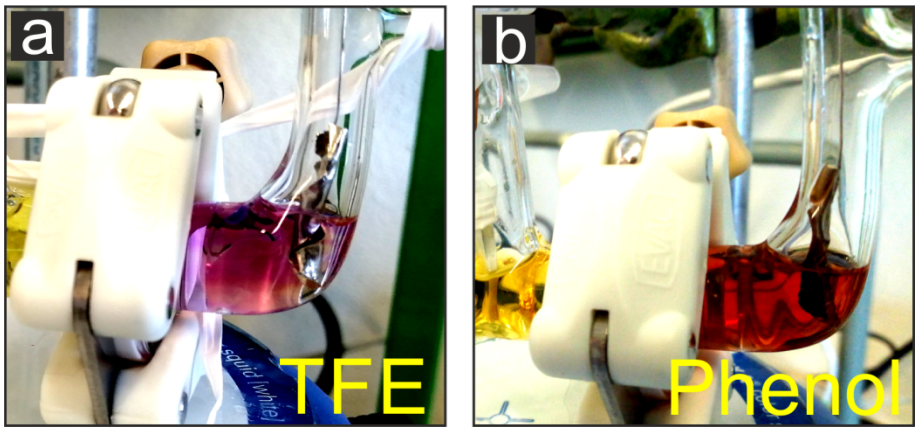

Figure S36. Photographs of the anolyte chamber after CO_2 reduction at –1.9 V *vs* Ag/AgCl for 2 h showing color changes in the anolyte when TFE (a) or phenol (b) are used as the proton donors, suggesting an anodic reaction of $(Bu_4N)PF_6$ as the electrolyte.

Table S11. Performance of different catalytic systems in electrochemical CO_2 reduction

Ni system	FE_{HCOO^-}	FE_{CO}	FE_{H2}	$E_{Applied}$	Solvent(s)	References
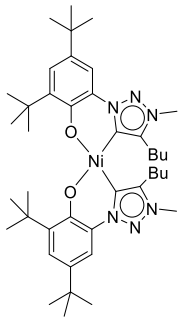	82%	<1%	3%	–1.9 V	MeCN	this work
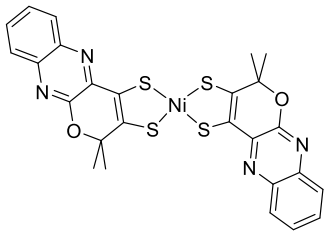	60%	19%	9%	–1.8V	MeCN/TFE [a)]	S17
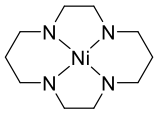	n.d.	90 %	n.d.	–1.2 V	MeCN/H_2O	S18
	75%	24%	n.d.	–1.4 V	DMF [b)]	

[a)] Trifluoroethanol (TFE); [b)] Dimethylformamide (DMF). *E*° referenced to Ag/AgCl for ref S17, while for ref S18 numbers were adapted from SCE using the formula V(Ag/AgCl) = V(SCE) + 0.045 V.[S19]

7. Electrode surface characterisation after electrolysis experiments

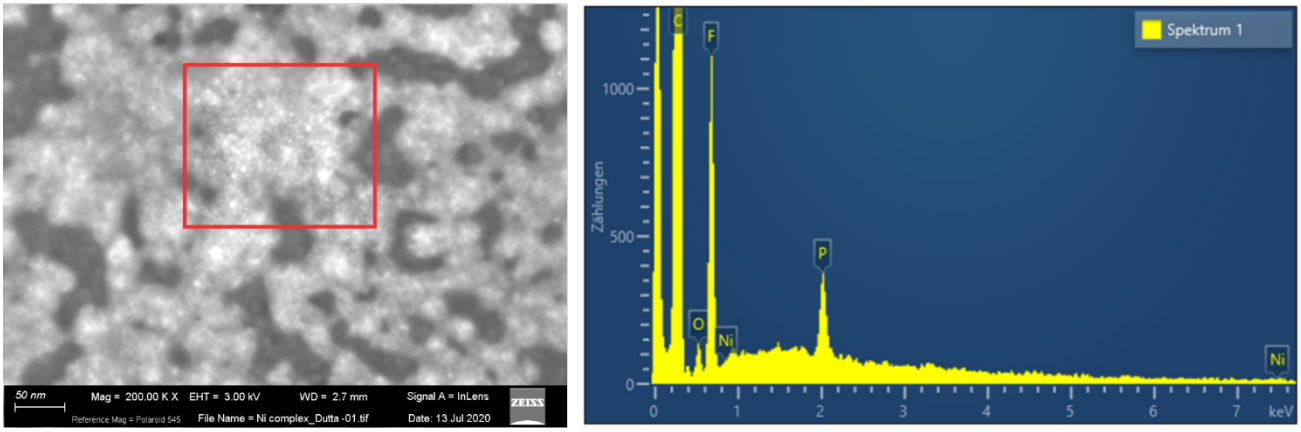

Figure S37. HRSEM image and EDX plot of the electrode surface after 2 h of electrolysis with complex **6b** at –1.9 V *vs* Ag/AgCl.

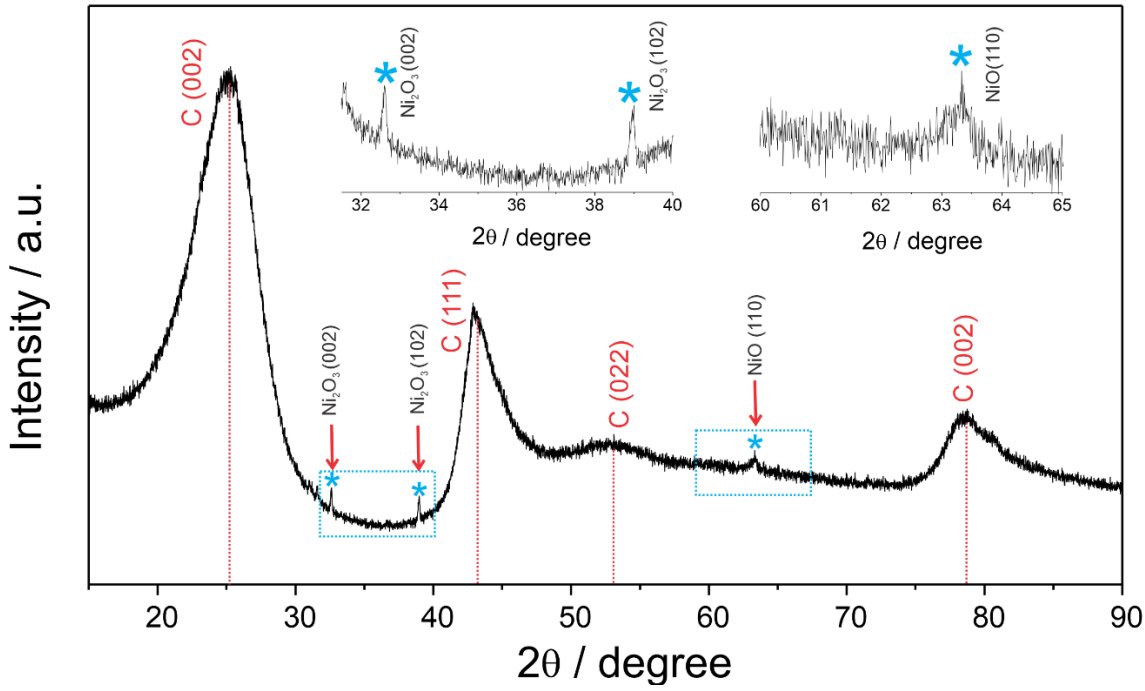

Figure S38. XRD characterization of the electrode surface after 2h of electrolysis with complex **6b** at –1.9 V *vs* Ag/AgCl.

8. References

S1 (a) Dulong, F.; Bathily, O.; Thuery, P.; Ephritikhine, M.; T. Cantat, T. *Dalton Trans*. **2012**, *41*, 11980 – 11983. (b) Liu, M.; M. Nieger, M.; Habner, E. G.; Schmidt, A. *Chem. Eur. J.* **2016**, *22*, 5416–5424. (c) Kotovshchikov, Y. N.; Latyshev, G. V.; Navasardyan, M. A.; Erzunov, D. A.; Beletskaya, I. P.; Lukashev, N. V. *Org. Lett.* **2018**, *20*, 4467–4470.

S2 Oxford Diffraction (2010). *CrysAlisPro* (Version 1.171.38.41). Oxford Diffraction Ltd., Yarnton, Oxfordshire, UK.

S3 Macchi, P.; Bürgi, H. B.; Chimpri, A. S.; Hauser, J.; Gál, Z. *J. Appl. Crystallogr.* **2011**, *44*, 763–771.

S4 Sheldrick, G. M *Acta Cryst*. **2015**, *A71*, 3 –8.

S5 Sheldrick, G. M. *Acta Cryst.* **2015**, *C71*, 3 –8.

S6 Yang, L.; Powell, D. R.; Houser, R. P. *Dalton Trans.* **2007***, 9,* 955 –964

S7 Connelly, N. G.; Geiger, W. E. *Chem. Rev.* **1996**, *96*, 877−910.

S8 Savéant, J.-M.; Su, K. B. *J. Electroanal. Chem*. **1984**, *171*, 341− 349.

S9 Delahay, P.; Stiehl, G. L. *J. Am. Chem. Soc*. **1952**, *74*, 3500− 3505.

S10 Schwarz, W. M.; Shain, I. *J. Phys. Chem*. **1965**, *69*, 30−40.

S11 Nicholson, R. S.; Shain, I. *Anal. Chem*. **1964**, *36*, 706−723.

S12 Savéant,J.-M.; Vianello, E. *Electrochim. Acta* **1967**, *12*, 629−646

S13 Andrieux, C. P.; Blocman, C.; Dumas-Bouchiat, J. M.; M'Halla, F.; Savéant, J.-M. *J. Electroanal. Chem*. **1980**, *113*, 19−40

S14 Savéant, J.-M.; Su, K. B. *J. Electroanal. Chem*. **1985**, *196*, 1−22.

S15 Costentin, C.; Drouet, S.; Passard, G.; Robert, M.; Savéant, J.-M. *J. Am. Chem. Soc*. **2013**, *135*, 9023−9031.

S16 Rahaman, M.; Dutta, A.; Broekmann, P. *ChemSusChem* **2017**, *10*, 1733 –1741

S17 T. Fogeron, T.; Todorova, T. K.; Porcher, J.-P.; Gomez-Mingot, M.; Chamoreau, L-M.; Mellot-Draznieks, C.; Li, Y.; Fontecave, M. *ACS Catal*. **2018**, *8*, 2030−2038

S18 (a) Collin, J.-P.; Jouaiti, A.; Sauvage, J.-P. *Inorg. Chem*. **1988**, 27, 1986 –1990. (b) Beley, M.; Collin, J. P.; Ruppert, R.; Sauvage, J.-P. *J. Chem. Soc., Chem. Commun*. **1984**, 1315−1316. (c) Froehlich , J. D.; Kubiak, C. P. *Inorg. Chem*. **2012**, 51, 3932–3934

S19 Sawyer, D. T.; Sobkowiak, A. J.; Roberts., J. *Electrochemistry for Chemists*, Second Edition, **1995**, John Wiley & Sons, NY.